Multiscale models for Light-Driven Processes

Michele Nottoli, Lorenzo Cupellini, Filippo Lipparini, Giovanni Granucci, Benedetta Mennucci*

Dipartimento di Chimica e Chimica Industriale, Università di Pisa, Via G. Moruzzi 14, 56124 Pisa, Italy; email: benedetta.mennucci@unipi.it

xxxxxx 0000. 00:1–36

Keywords

QM/MM, continuum models, nonadiabatic dynamics, multichromophoric systems, excitation energy transfer, electron transfer

Abstract

Multiscale models combining quantum mechanical and classical descriptions are a very popular strategy to simulate properties and processes of complex systems. Many alternative formulations have been developed in the last decades and they are now available in all the most widespread quantum chemistry packages. Their application to the study of light-driven processes, however, is more recent and some methodological and numerical problems are still to be solved. This is especially the case for the polarizable formulation of these models, of which we review here the recent advances. In particular, we identify and describe the most important specificities that the polarizable formulation introduces in the simulation of excited state dynamics and in the modeling of excitation energy and electron transfer processes.

Contents

1. INTRODUCTION

Light is the trigger for many important biological processes, such as photosynthesis and vision, just to cite the most widely known. Understanding how light is sensed and used by various organisms is clearly of paramount importance for improving our knowledge of the natural world. As a matter of fact, achieving a molecular-level picture of light-driven processes could allow us to go beyond the "stage of understanding", and lead the way in using light as a tool to control and tune natural processes, for example for medical purposes, as well as to design artificial devices for selected applications.

By definition, a molecular-level description of light-driven processes should be achievable applying the proper quantum chemical approach. However, the many space and time scales involved make this logical strategy unfeasible for realistic systems. A possible solution to this apparently insurmountable limit is to introduce a multiscale strategy where quantum mechanical (QM) and classical (C) models mix and merge to give a new hybrid framework able to cope with multiple time and space scales. This hybrid QM/C framework is neither unique nor perfect. Many different alternatives have been proposed so far, each one having its own drawbacks and limitations. Nevertheless, up to now, it still represents the most effective approach to investigate the response of (bio)systems to light, from the initial electronic excitation, to energy/charge transfers and photochemical reactions.

The idea of coupling QM and classical descriptions dates back to the 70s of the last century (1–3) and during these almost 50 years many models have been proposed. Nowadays it is common to collect them depending on the coarseness used to describe the classical part of the system. Within this framework, the continuum versus discrete (or atomistic) antithesis is commonly introduced. In the former case, the classical part loses any atomistic detail and becomes a continuum medium characterized by selected macroscopic properties, among which the most important is the dielectric permittivity (4–7). In the latter case, instead, the atomic details of the classical part remain, but the atoms and their interactions are recast in a classical picture, commonly by introducing a Molecular Mechanics (MM) force field (8–11).

The continuum formulation does not require any model for describing the interactions

within the classical part but only a representation of its effect on the QM part. This is commonly achieved by introducing a closed boundary between the QM and the classical parts which defines the surface of the molecular cavity containing the QM system. This boundary allows one to represent the polarization induced by the QM system into the classical part, seen as a dielectric medium, as an apparent surface charge (ASC) distribution (6, 7). In the numerical implementation of continuum models, this charge distribution is commonly discretized into point charges, one for each of the finite elements (also known as "tesserae" in the jargon of continuum models) of the mesh used to represent the cavity surface. These point charges are finally used to define a QM operator to be added to the Hamiltonian of the QM subsystem to include its interaction with the environment.

Similarly, in the most popular formulation of discrete models, the QM subsystem feels the classical part as a set of point charges. This time, however, the point charges are parameters defined by the specific MM force field selected for representing the classical subsystem. This formulation is commonly indicated as electrostatic embedding (EE) QM/MM. The resulting QM operator to be added to the Hamiltonian of the QM subsystem is defined exactly as for ASC-like continuum models. However, the nature of the charges is completely different, as in EE QM/MM they represent the atoms of the MM system, while in QM/continuum they are a numerical representation of the polarization of the dielectric medium. This difference is reflected in the fact that the MM charges exist independently from the QM subsystem, they have fixed values, and their positions are determined by the position of the MM atoms. On the contrary, the ASCs are induced by the QM subsystem and their positions are linked to the the positions of the QM atoms through the cavity surface. It is clear that ASC-like continuum models automatically include mutual polarization effects between the QM and the classical subsystems, while this is not the case for EE QM/MM approaches. In order to recover the effects of mutual polarization, the EE embedding has to be changed so to include polarizable sites in the MM part. This can be obtained in different ways: the most popular ones are those based on a Drude oscillator, a fluctuating charge or an induced point dipole (IPD) model (12–19). A different strategy, which avoids the introduction of parametrized force fields, relies on QM-based potentials, also known as non-empirical polarizable potentials. Among them, the Effective Fragment Potential (EFP) method (20–22) and the explicit polarization (X-Pol) model (23, 24) are the most popular ones.

A polarizable formulation is expected to be better suited to describe the response of the environment in light-driven processes, where the electronic transitions and the following transformations involved require a model flexible enough to be applicable within a temporal multiscale framework. For that reason, the present review is focused on the polarizable formulation of the hybrid QM/C strategy. Moreover, such polarizable formulation can be easily reduced to the non-polarizable one (while the opposite is not straightforward) and this allows us to present a single general formalism.

This review is organized as follows. We start by describing the main methodological aspects of polarizable hybrid approaches for ground and excited state systems (Section 2), and then we move to describe their extension to (non)adiabatic methods to simulate excited state dynamics (Section 3). Finally, in Section 4, we present an alternative formulation based on model Hamiltonians which approximate the nuclear degrees of freedom of the system as quantum harmonic oscillators. For both types of approaches some examples of application to selected light-driven processes are given. In particular, for the methods explicitly simulating the nuclear motions either within an adiabatic or nonadiabatic frame-

work, the focus will be on excited state proton transfer and singlet fission, while for vibronic models the examples of excitation energy transfer and electron transfer will be presented and discussed. We note that, in this review, we have deliberately neglected the application of multiscale methods to optical spectroscopies and important photochemical reactions such as photoisomerization and photodissociations, and we have paid little attention to photoinduced processes in materials. The reason for this choice is that the field of light-driven processes is too large to be fully investigated in a single review and an arbitrary selection is unavoidable. Moreover, comprehensive reviews on these and other aspects of multiscale methods for photo-induced processes which are not discussed here have recently appeared in the literature (25–33): the interested reader can refer to them to complement the present selection of methods and processes.

2. HYBRID QM/C STRATEGY: THE POLARIZABLE FORMULATION

In this section, we develop a general formalism for the hybrid QM/C strategy which includes a classical polarizable model either at a continuum or atomistic level. The discussion is focused on the description of the ground state of an embedded molecule described at a self-consistent field (SCF) level of theory, such as Hartree-Fock (HF) or Kohn-Sham (KS) Density Functional Theory (DFT). In order to keep the notation simple, all the equations are given for the HF model, but a generalization to DFT is straightforward.

2.1. A general, variational formalism for polarizable models

In a general framework, the embedded system can be described by means of three different charge distributions: the QM charge density ρ, a fixed distribution of classical charges or higher order multipoles $\mathbf{M}$, and a polarizable charge distribution $\mathbf{X}$. To clarify this point, let us consider two examples (Figure 1). For an IPD-based polarizable QM/MM method (1, 34–37), or, with little variations, for Drude oscillators polarizable QM/MM (38–40), besides the QM density, each MM atom is commonly endowed with a point charge and with a polarizability. Therefore, $\mathbf{M}$ is a collection of point charges placed at the positions of the MM atoms, while $\mathbf{X}$ is a set of IPD at the polarizable MM atoms. For a continuum solvation model, there is no fixed electrostatic distribution, so $\mathbf{M} = 0$ and $\mathbf{X}$ is the ASC distribution (6).

We assume that all the charge distributions interact classically and that the interaction energy is bi-linear with respect to pairs of distributions. In general, we write

$$E^{\text{int}}(\rho, \mathbf{M}) = \langle \Phi(\rho), \mathbf{M} \rangle, \quad E^{\text{int}}(\rho, \mathbf{X}) = \langle \Psi(\rho), \mathbf{X} \rangle, \quad E^{\text{int}}(\mathbf{M}, \mathbf{X}) = \langle \Psi(\mathbf{M}), \mathbf{X} \rangle, \quad (1)$$

where Φ and Ψ are appropriate, model-dependent linear functionals of the distributions. In this section, we also assume that the polarization degrees of freedom are the minimizers of a variational energy functional (41). This is indeed the case for most polarizable models, with a few notable exceptions, such as the QM/AMOEBA (36, 42) and QM/ddCOSMO (43) models. A generalization to non variational models can be found elsewhere (44). The variational assumption translates into the fact that the polarization degrees of freedom $\mathbf{X}$ are obtained by solving a linear set of equations

$$\mathbf{A}\mathbf{X} = \Psi(\rho) + \Psi(\mathbf{M}), \quad (2)$$

where $\mathbf{A}$ is a symmetric, positive definite linear operator (or a matrix) and Ψ is the same

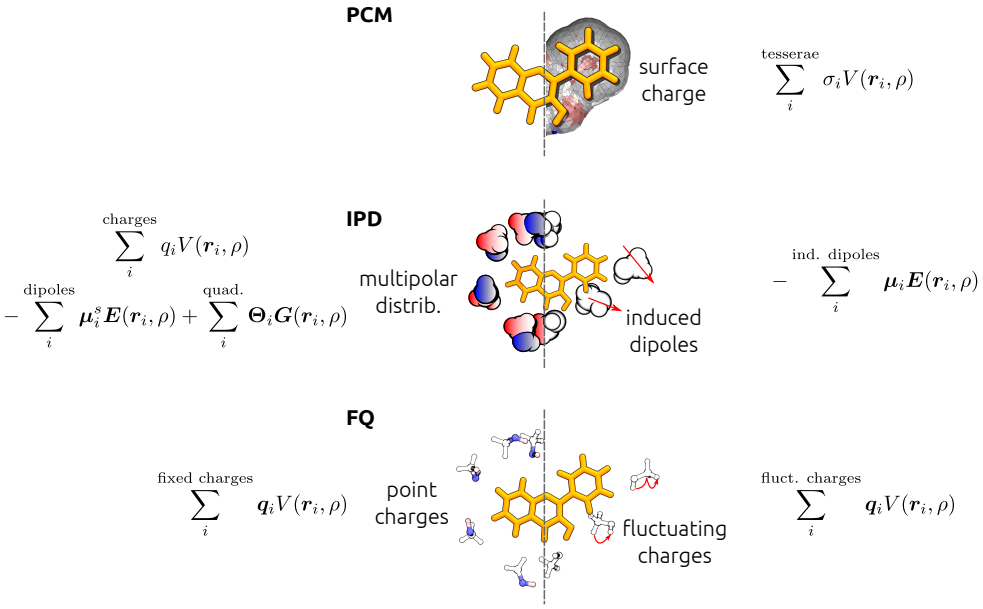

Figure 1

Charge distributions for three multiscale models. Orange: QM molecule bearing the QM charge distribution (ρ). Left: fixed charge distributions ($\mathbf{M}$) and expressions for their interaction with ρ, right: induced charge distributions ($\mathbf{X}$) and expressions for their interaction with ρ.

linear functional of the sources defined above. This allows us to write the total energy as

$$\mathcal{E}(\rho, \mathbf{X}; \mathbf{M}) = E^{\text{QM}}(\rho) + E^{\text{self}}(\mathbf{M}) + \langle \Phi(\rho), \mathbf{M} \rangle + \frac{1}{2}\langle \mathbf{X}, \mathbf{A}\mathbf{X} \rangle + \langle \Psi(\rho), \mathbf{X} \rangle + \langle \Psi(\mathbf{M}), \mathbf{X} \rangle, \quad (3)$$

where $E^{\text{self}}(\mathbf{M})$ is the coulomb interaction of the static sources with themselves and the term $\frac{1}{2}\langle \mathbf{X}, \mathbf{A}\mathbf{X} \rangle$ accounts for the work required to polarize the system.

It has to be noted that some polarization models, such as the fluctuating charge (FQ) model (45, 46), require one to perform a constrained minimization with respect to the polarization degrees of freedom, for instance, in order to enforce the total charge of the system or of a fragment. This is easily implemented using Lagrange multipliers, i.e., by adding to the energy functional in eq. 3 a term

$$\langle \Lambda, \mathbf{C}\mathbf{X} \rangle, \quad (4)$$

where we assume that the constraints are linear. By optimizing the global energy functional with respect to both the polarization degrees of freedom and the Lagrange multipliers, the polarization equations are obtained and one can use the variational formalism presented in the following with little modification.

The notation defined here is completely general. In order to better clarify it, let us reconsider the two starting examples. Figure 1 provides a graphical representation of the fixed and induced densities, as well as the expression of the interaction between the classical and QM densities. For an IPD-based QM/MM model ($X_i = \mu_i$) where a fixed distribution

of charges ($M_i = q_i$) is also present, we have

$$\Phi_i(\rho) = \Phi(\mathbf{r}_i)(\rho) = \int \frac{\rho(\mathbf{r})}{|\mathbf{r} - \mathbf{r}_i|} d^3r, \quad \langle \Phi(\rho), \mathbf{M} \rangle = \sum_i q_i \Phi_i(\rho), \tag{5}$$

i.e., $\Phi(\rho)$ is the electrostatic potential generated by the QM distribution,

$$\Psi_i(\rho) = \Psi(\mathbf{r}_i)(\rho) = \int \frac{\rho(\mathbf{r})(\mathbf{r} - \mathbf{r}_i)}{|\mathbf{r} - \mathbf{r}_i|^3} d^3r, \quad \langle \Psi(\rho), \mathbf{X} \rangle = -\sum_i \mu_i \Psi_i(\rho), \tag{6}$$

i.e., $\Psi(\rho)$ is the electric field generated by ρ and, analogously,

$$\Psi_i(\mathbf{M}) = \sum_j \frac{q_j(\mathbf{r}_j - \mathbf{r}_i)}{|\mathbf{r}_j - \mathbf{r}_i|^3} d^3r, \quad \langle \Psi(\mathbf{M}), \mathbf{X} \rangle = -\sum_i \mu_i \Psi_i(\mathbf{M}). \tag{7}$$

Furthermore,

$$E^{\text{self}}(\mathbf{M}) = \frac{1}{2} \sum_{i \neq j} \frac{q_i q_j}{|\mathbf{r}_i - \mathbf{r}_j|} \tag{8}$$

and

$$\frac{1}{2} \langle \mathbf{X}, \mathbf{A}\mathbf{X} \rangle = \frac{1}{2} \left(\sum_i \alpha_i^{-1} \mu_i^2 + \sum_{i \neq j} \mu_i T_{ij} \mu_j \right), \quad T_{ij} = \frac{1}{|\mathbf{r}_i - \mathbf{r}_j|^3} - 3 \frac{(\mathbf{r}_i - \mathbf{r}_j) \otimes (\mathbf{r}_i - \mathbf{r}_j)}{|\mathbf{r}_i - \mathbf{r}_j|^5}, \tag{9}$$

where α_i is the polarizability of site i, and T_{ij} is the interaction tensor between dipoles i and j.

For a continuum solvation model (CSM) such as the conductor-like screening model (47), the polarization degrees of freedom are the expansion coefficients q_i of an apparent surface charge discretized using a set of functions $\sigma_i(\mathbf{r})$ (usually, piecewise constant or spherical Gaussians (48)) placed at representative points $\mathbf{s}_i$. With slight variations depending on the implementation, we have

$$\Psi_i(\rho) = \Psi(\mathbf{s}_i)(\rho) = -\int \frac{\rho(\mathbf{r})\sigma_i(\mathbf{r})}{|\mathbf{r} - \mathbf{s}_i|} d^3r, \tag{10}$$

$$\frac{1}{2} \langle \mathbf{X}, \mathbf{A}\mathbf{X} \rangle = \frac{1}{2} \sum_{i,j} q_i S_{ij} q_j, \quad S_{ij} = \int d^3r \int d^3r' \frac{\sigma_i(\mathbf{r})\sigma_j(\mathbf{r}')}{|\mathbf{r} - \mathbf{r}'|}. \tag{11}$$

In both cases, we note that the energy functional in eq. 3 is indeed a variational functional of the polarization degrees of freedom $\mathbf{X}$, i.e., the polarization equations are satisfied when the functional is minimized (41)

$$\frac{\partial \mathcal{E}(\rho, \mathbf{M}, \mathbf{X})}{\partial \mathbf{X}} = \mathbf{A}\mathbf{X} - \Psi(\rho) - \Psi(\mathbf{M}) = 0 \tag{12}$$

This has an important advantage, as it makes computing analytical derivatives of the energy straightforward. In fact, for a generic parameter ξ, we get

$$\frac{dE^{\text{pol}}}{d\xi} = \frac{\partial E^{\text{pol}}}{\partial \xi} + \frac{\partial E^{\text{pol}}}{\partial \mathbf{X}} \frac{\partial \mathbf{X}}{\partial \xi} = \frac{\partial E^{\text{pol}}}{\partial \xi}, \tag{13}$$

where the partial derivative denotes explicit derivatives only.

2.2. Polarizable embedding at the self-consistent field level of theory

The formalism developed in section 2.1 can be used in a straightforward way to derive the coupled QM/C equations when the QM portion of the system is described at a level of theory based on the self-consistent field method (49). Let us introduce a basis set of atomic orbitals (AO) χ. The QM density can be expanded as

$$\rho(\mathbf{r}) = \sum_{\alpha} Z_{\alpha}\delta(\mathbf{r}-\mathbf{R}_{\alpha}) - \sum_{\mu\nu} P_{\mu\nu}\chi_{\mu}(\mathbf{r})\chi_{\nu}(\mathbf{r}), \tag{14}$$

where the first term accounts for the nuclear charges and $\mathbf{P}$ is the idempotent density matrix, namely $\mathbf{P} = \mathbf{C}_{\mathrm{occ}}\mathbf{C}_{\mathrm{occ}}^{\dagger}$, where $\mathbf{C}_{\mathrm{occ}}$ is the occupied block of the molecular orbitals (MO) coefficients matrix $\mathbf{C}$.

In order to write the coupled HF/PE equations, let us first express the quantities Φ and Ψ in terms of ρ. As both these quantities are linear functionals of the total density, they can be written as the sum of a nuclear contribution plus an electronic one. The latter can in turn be written as the contraction of the density matrix with the appropriate one-electron integrals $\Phi_{\mu\nu}$ and $\Psi_{\mu\nu}$ that are obtained by substituting in the model-specific definition of Φ and Ψ the elementary density element $\chi_{\mu}(\mathbf{r})\chi_{\nu}(\mathbf{r})$ to the total density $\rho(\mathbf{r})$:

$$\Phi(\rho) = \Phi^{\mathrm{nuc}} + \sum_{\mu\nu} P_{\mu\nu}\Phi_{\mu\nu}; \quad \Psi(\rho) = \Psi^{\mathrm{nuc}} + \sum_{\mu\nu} P_{\mu\nu}\Psi_{\mu\nu} \tag{15}$$

Coupled HF/Polarizable environment equations are obtained exploiting the fact that the total energy functional

$$\mathcal{E}(\mathbf{P},\mathbf{X};\mathbf{M}) = E^{\mathrm{HF}}(\mathbf{P}) + E^{\mathrm{self}}(\mathbf{M}) + \langle\Phi(\mathbf{P}),\mathbf{M}\rangle + \frac{1}{2}\langle\mathbf{X},\mathbf{A}\mathbf{X}\rangle + \langle\Psi(\mathbf{P}),\mathbf{X}\rangle + \langle\Psi(\mathbf{M}),\mathbf{X}\rangle \tag{16}$$

is variational in both the density matrix $\mathbf{P}$ and the polarization degrees of freedom. Imposing the stationarity conditions with respect to $\mathbf{P}$ and taking into account the constraints gives a set of modified Roothan equations

$$\tilde{\mathbf{F}}(\mathbf{P})\mathbf{C} = \mathbf{S}\mathbf{C}\mathbf{E} \tag{17}$$

with a modified Fock matrix

$$\tilde{F}_{\mu\nu} = \frac{\partial\mathcal{E}(\mathbf{P},\mathbf{X};\mathbf{M})}{\partial P_{\mu\nu}} = h_{\mu\nu} + G_{\mu\nu}(\mathbf{P}) + \langle\mathbf{M},\Phi_{\mu\nu}\rangle + \langle\mathbf{X},\Psi_{\mu\nu}\rangle. \tag{18}$$

The polarization equations are instead obtained by imposing the stationarity conditions with respect to $\mathbf{X}$

$$\frac{\partial\mathcal{E}(\mathbf{P},\mathbf{X};\mathbf{M})}{\partial\mathbf{X}} = \mathbf{A}\mathbf{X} - \Psi(\mathbf{P}) - \Psi(\mathbf{M}) = 0. \tag{19}$$

We note immediately that the two sets of equations 17 and 19 are coupled, as the former depends on $\mathbf{X}$ and the latter on $\mathbf{P}$. In practical implementations, the polarization equations need to be solved at each SCF cycle, so that the Fock matrix can be updated. The total energy is obtained by substituting the solutions to the coupled equations into the variational energy functional. We note that the polarization terms simplify to

$$E^{\mathrm{pol}} = \frac{1}{2}\langle\Psi(\mathbf{P}) + \Psi(\mathbf{M}),\mathbf{X}\rangle. \tag{20}$$

2.3. Beyond the SCF description: the modeling of excited states

As shown in section 2.2, the coupling of polarizable methods to HF or DFT can be achieved in an univocal, rigorous way thanks to the use of a variational formalism. Unfortunately, this is not the case for virtually any other quantum chemical method, with the only excpection of state-specific multiconfigurational SCF, for which an analogous variational energy functional can be defined. In this section, we will illustrate what are the main approaches to couple polarizable methods to the description of excited states

2.3.1. Linear response schemes. Excited states and transition properties can be successfully described in terms of linear response (LR) theory which, combined with a SCF QM description, gives rise to the so-called time-dependent SCF equations(50). In vacuo, at the HF level of theory, such equations read

$$\begin{pmatrix} A & B \\ B^* & A^* \end{pmatrix} \begin{pmatrix} X \\ Y \end{pmatrix} = \omega \begin{pmatrix} 1 & 0 \\ 0 & -1 \end{pmatrix} \begin{pmatrix} X \\ Y \end{pmatrix} \tag{21}$$

where the A and B matrices are given by

$$\begin{aligned} A_{ia,jb} &= \delta_{ij}\delta_{ab}(\epsilon_a - \epsilon_i) + (ia|jb) - (ab|ij) \\ B_{ia,jb} &= (ia|jb) - (aj|ib) \end{aligned} \tag{22}$$

where i, j are the indices of occupied molecular orbitals, and a, b of virtual molecular orbitals, ϵ_i are the molecular orbital energies, and $(ai|bj)$ is a bielectronic integral in the Mulliken notation.

When a polarizable environment is included, the LR equations can be derived starting from the variational energy functional following the same procedure used in vacuo (51, 52). However, the equations one obtains account for the presence of the environment in a fundamental way, as the response matrix is modified with an additional term that accounts for a dispersion-like polarization contribution. In particular, the A and B matrices in eq. 21 are modified as follows:

$$\tilde{A}_{ia,jb} = A_{ia,jb} + \mathcal{V}^{\text{env}}_{iajb}, \quad \tilde{B}_{ia,jb} = B_{ia,jb} + \mathcal{V}^{\text{env}}_{iajb}, \tag{23}$$

where

$$\mathcal{V}^{\text{env}}_{iajb} = \langle \Psi_{ia}, X_{jb} \rangle \tag{24}$$

and X_{jb} is the polarization induced by the field Ψ_{jb} arising from orbitals $\phi_j\phi_b$. In other words, the polarizable environment contributes to the molecular response properties and excitation energies with a term $\langle X^K, \Psi^K(\rho^K)\rangle$, where ρ^K is the transition density between the ground and the K-th excited states and X^K the polarization induced by such a density. We note that if the polarizable environment response has a (non-negligible) frequency dependence, as it is the case for continuum solvation models, this can be easily accounted for in a LR treatment, as one can use the zero-frequency limit of the response for the ground state polarization equations and the optical limit for the linear response ones. This approach, known as non-equilibrium solvation in CSM, is nowadays routinely implemented and used (53).

The LR treatment of embedded systems is sound and rigorous, however, it represents only a part of the whole effect of a polarizable environment. In fact, the missing term is

the relaxation of the polarization in response to the change in the charge density of the QM subsystem upon an electronic transition (54–56). This further effect, which is expected to be large any time the excitation induces a large electronic charge redistribution such as in charge-transfer excitations, requires a different formulation with respect to the LR framework. In particular, the response of the environment to the excitation now becomes specific to the involved excited state and as such it has been commonly described as state-specific (SS) formulation. The main theoretical and methodological aspects of such formulation will be summarized in the next section.

2.3.2. State-specific schemes. Several SS alternatives have been developed over the years, which introduce a coupling between the excited state density and the environment at different levels of approximation (51, 57, 58).

SS models have the attractive feature that they achieve mutual polarization in their description of the embedded system, however, they also exhibit a number of relevant problems (59). First, they are computationally expensive. In fact, they require one to assemble the state or relaxed one-body density matrix several times, until self-consistent polarization is reached. In LR calculations, there is no need to compute such a density (58). To make an example, in a DFT SS calculation, computing the relaxed density requires one to solve the Z-vector equations, which comes with a cost similar to the one associated with solving the linear response equations. Then, the density has to be assembled, a new response of the environment computed and the process repeated until convergence. Assuming that one needs 5-10 iterations to converge, the overall calculation will be 10-20 times more expensive than the corresponding LR one.

A second problematic factor concerns more theoretical aspects of such models. The polarizable environment introduces in fact a density-dependent term in the molecular Hamiltonian, making thus the approximate solution to the electronic Schrödinger equation a non-linear problem. This is in contrast with the linear nature of the response equations and introduces several difficulties. First, the transition and relaxation contributions to the density become non-linearly coupled, which blurs the clear-cut distinction between such quantities (60). If the SCF orbitals are recomputed, things become even more unclear from a theoretical point of view, as the ground state orbitals become coupled to the excited state densities (57). These problems become even more substantial if one adopts a post-SCF description for the excited state (61), for instance, using Coupled-Cluster theory, as a fully self-consistent procedure couples the amplitude and Λ equations to the left and right eigenvector equations that one needs to solve in order to compute the excited state density (61).

Second, the embedded electronic state obtained in a SS approach is not orthogonal to the ground state, nor to any other excited state obtained with the same procedure. This is a major theoretical problem, as it blurs again the definition itself of excited state in a quantum mechanical sense.

A particularly interesting case is offered by the description of excited states in a polarizable environment using a multiconfigurational SCF (MCSCF) approach (62–64). MCSCF methods grant in principle a direct access to excited states, that can be obtained by selecting a specific root of the CI problem. In general, there are two approaches to compute excited-state wavefunctions with such a method. A single root can be completely optimized, obtaining thus both molecular orbitals and CI coefficients specifically for the desired state, or several roots can be optimized at once, at the price of using state-averaged (SA)

molecular orbitals. The latter approach has the advantage of producing more states at the same time, and that such states are orthonormal. On the other hand, the common set of molecular orbitals might not be particularly well suited for the description of all the states at once, especially if such states involve large rearrangements of the electronic density. In contrast, the single-state approach provides a fully optimized excited state wavefunction. However, it may suffer of convergence issues for higher lying excited states and different states obtained with this method are no longer orthogonal. A linear response formalism can also be applied at the MCSCF level of theory in order to study excitation processes (65).

As the MCSCF wavefunction is obtained via a non-linear optimization procedure, the further non-linearity introduced by polarizable models is neither a theoretical nor a practical limitation. Therefore, the single-state MCSCF method can be combined with polarizable methods (62) in a genuinely SS fashion. This comes, however, with all the limitations discussed before, in particular, the lack of orthogonality between different states. Embedded approaches based on SA or LR MCSCF can also be formulated and implemented (63, 64). In this case, several orthogonal states can be obtained, but the response of the environment will be either incomplete for linear response, or averaged for SA, which can be physically questionable. A more specific problem is encountered when SA methods are used in order to explore a potential energy surface via a molecular dynamics simulation, which requires energy gradients. Here the SS approach is simpler, as it is fully variational. On the other hand, a SA approach requires one to introduce a Lagrangian and solve coupled perturbed equations in order to compute the state energy gradients (66). A possible way of overcoming such problems is to approximate the QM/C coupling in order to remove crossed dependencies. As an example, in the corrected LR (cLR) approach (51), the excited state density is used to correct the energy in a state-specific way, but the density is left unchanged. This is a compromise that can improve the energy, but not the transition or state properties, and it is computationally much less expensive than a fully polarized SS approach. The cLR approach can be also applied to SA MCSCF descriptions. In this case, a state-specific polarization energy is computed and used to correct the state energy (64).

It should be mentioned that the difference between LR and SS approaches, and the issues encountered with such methods, are more prominent in continuum solvation models than in polarizable MM ones. This is due to the fact that in the latter polarization represents a (small) fluctuation of the electrostatic distribution of the environment with respect to its equilibrium one, which is mostly represented by the static multipolar distribution $\mathbf{M}$. As $\mathbf{M}$ is not present in CSM, the whole interaction is represented as a polarization term. As polarization is the only part that introduces a non-linearity in the Hamiltonian, this problem is much more severe for CSM. In view of these problems, a polarizable approach that allows one to obtain more states at the same time, while introducing state-specific corrections and retaining a clear-cut interpretation of the states from a QM point of view is nowadays still not available.

2.3.3. Analytical Gradients. The discussion in the current section has been entirely focused on the calculation of the energy of ground and excited states embedded in a polarizable environment. However, the applicability of polarizable methods to the study of light-driven, dynamical processes requires one to be able to explore a potential energy surface, which in turn requires the availability of analytical gradients. The presence of a polarizable environment changes the calculation of the forces for both ground and excited states. Here

we present an example of how these changes can be included within a linear response formulation using the formalism presented in Section 2. The variational formalism makes the derivation of gradients particularly straightforward, as the energy functional that has to be differentiated is stationary with respect to the polarization degrees of freedom, making thus all the chain-rule derivatives with respect to $\mathbf{X}$ vanish.

We start with the GS contribution by taking the derivative of eq. 16 with respect to the position of QM atoms (R) and MM atoms (r).

$$\nabla_R \mathcal{E}(\rho, \mathbf{X}; \mathbf{M}) = \nabla_R E^{\mathrm{QM}}(\rho) + \langle \nabla_R \Phi(\rho), \mathbf{M} \rangle + \langle \nabla_R \Psi(\rho), \mathbf{X} \rangle \tag{25}$$

$$\begin{aligned} \nabla_r \mathcal{E}(\rho, \mathbf{X}; \mathbf{M}) = \nabla_r E^{\mathrm{self}}(\mathbf{M}) + \langle \nabla_r \Phi(\rho), \mathbf{M} \rangle + \frac{1}{2} \langle \mathbf{X}, \nabla_r \mathbf{A} \mathbf{X} \rangle \\ + \langle \nabla_r \Psi(\rho), \mathbf{X} \rangle + \langle \nabla_r \Psi(\mathbf{M}), \mathbf{X} \rangle \end{aligned} \tag{26}$$

The first expression contains the purely QM gradients and two additional contributions coming from the derivative of the interactions between $\mathbf{X}$ and $\mathbf{M}$ and the quantum density ρ. The second expression contains the purely classical electrostatic forces — sum of three terms, and again two contributions from the derivative of the interactions between the quantum density and the classical densities $\mathbf{X}$ and $\mathbf{M}$. Note that in eq. 25 the Ψ and Φ functions are derived with respect to the sources and in eq. 26 with respect to the targets, leading to different expressions. Eq. 26 accounts only for the electrostatic and polarization contributions to the classical gradients, since $\mathcal{E}$ is the sum of the QM energy and the polarization and electrostatic energy. Other contributions, such as dispersion-repulsion and bonded terms, are needed to assemble the total gradients, but they are specific of the model and not discussed here. Furthermore, such contributions are usually modeled using a classical, additive potential and pose therefore little to no theoretical problem.

The gradients of a given excited state energy are the sum of the GS gradients and an additional contribution due to the derivatives of the excitation energy. In case of a linear response description, the latter term cannot be computed in a straightforward way, as the linear response energy is not stationary with respect to the MO coefficients. In order to avoid computing the derivatives of the MO coefficients, that would stem from various chain-rule terms, a linear response Lagrangian which is variational in the MO coefficients(67), is introduced and properties are obtained by its differentiation.

$$\begin{aligned} \mathcal{L} = \begin{pmatrix} \boldsymbol{X} & \boldsymbol{Y} \end{pmatrix} \begin{pmatrix} \boldsymbol{A} & \boldsymbol{B} \\ \boldsymbol{B}^* & \boldsymbol{A}^* \end{pmatrix} \begin{pmatrix} \boldsymbol{X} \\ \boldsymbol{Y} \end{pmatrix} - \omega \left[\begin{pmatrix} \boldsymbol{X} & \boldsymbol{Y} \end{pmatrix} \begin{pmatrix} \mathbf{1} & \mathbf{0} \\ \mathbf{0} & -\mathbf{1} \end{pmatrix} \begin{pmatrix} \boldsymbol{X} \\ \boldsymbol{Y} \end{pmatrix} - \mathbf{1} \right] \\ + \sum_{ia} Z_{ia} F_{ia} + \sum_{pq} W_{pq} (S_{pq} - \delta_{pq}) \end{aligned} \tag{27}$$

In eq. 27 the first two terms are the LR energy functional, the third term enforces the solution of the SCF equations and the fourth term enforces the orthonormality. Solving the SCF and LR equations provides the MO coefficients and the $\boldsymbol{X}$ and $\boldsymbol{Y}$ vectors, however the $\boldsymbol{Z}$ and $\boldsymbol{W}$ coefficients are still needed to build the Lagrangian, and thus its derivatives. The latter terms are computed by solving the so-called Z-vector equations, which are obtained by imposing the stationarity of eq. 27 with respect to the MO coefficients.

Properties can then be obtained by differentiation of the LR Lagrangian. We focus here on the terms induced by a multiscale description, by directly reporting their expression in

the AO basis. A detailed derivation can be found elsewhere(67, 68).

$$\nabla_R \mathcal{L}^{\text{env}} = \sum_{\mu\nu} P^{\Delta}_{\mu\nu} \nabla_R F_{\mu\nu} + \sum_{\mu\nu\kappa\lambda} P^{\text{tr}}_{\mu\nu} P^{\text{tr}}_{\kappa\lambda} 2\langle \nabla_R \Psi_{\mu\nu}, \mathbf{X}_{\kappa\lambda} \rangle \tag{28}$$

$$\nabla_r \mathcal{L}^{\text{env}} = \sum_{\mu\nu} P^{\Delta}_{\mu\nu} \nabla_r F_{\mu\nu} + \sum_{\mu\nu\kappa\lambda} P^{\text{tr}}_{\mu\nu} P^{\text{tr}}_{\kappa\lambda} (2\langle \nabla_r \Psi_{\mu\nu}, \mathbf{X}_{\kappa\lambda} \rangle + \langle \mathbf{X}_{\mu\nu}, \nabla_r \mathbf{A} \mathbf{X}_{\kappa\lambda} \rangle) \tag{29}$$

The expressions in eq. 29 contain two different contributions. The first depends on the so-called relaxed density difference $\boldsymbol{P}^{\Delta}$ and is analogous to the environment contribution to the GS gradients. It can therefore be computed by defining a total relaxed density matrix $\boldsymbol{P}^{\text{tot}} = \boldsymbol{P} + \boldsymbol{P}^{\Delta}$, and a total relaxed density $\rho^{\text{tot}}(\boldsymbol{P}^{\text{tot}})$ (as in eq. 14), which is then fed to same GS gradients routines (i.e., this term is evaluated with eqs. 25, 26) with ρ^{tot} in place of ρ. The second contribution is quadratic in the transition density $\boldsymbol{P}^{\text{tr}}$ and is specific to polarizable embedding schemes, which contribute explicitly to the LR equations.

Gradients of LR methods have been developed for several polarizable multiscale approaches, such as ASC models (68), fluctuating charges (69), IDP (70**?**), and, recently, for an embedding based on the AMOEBA force field (71).

We conclude this section mentioning approaches going beyond a SCF-based LR description for which analytical gradients are available. Deriving and implementing gradients for methods such as the ones described in Section 2.3.2 is not an easy task, so very few implementations are available. Due to the cost of computing the relaxed SS density, gradients are more commonly available for already expensive post Hartree–Fock methods, for which a state-specific formulation is available. We mention here, in the context of continuum models, the SS formulations at the equation-of-motion Coupled Cluster level of theory (72) and linear-response Coupled Cluster (73), and at the second-order adiabatic diagrammatic correction (ADC(2)) level (74). The latter level of theory has also been coupled to an IPD polarizable MM formulation (75). As mentioned in Section 2.3.2, MCSCF methods can naturally be coupled to a polarizable environment in a SS fashion. As the excited state energy is variational, the implementation of gradients does not suffer of any particular complications due to the presence of the embedding (34, 62), so that once standard SCF gradients have been implemented, the extension to MCSCF gradients is straightforward.

3. EXCITED STATE DYNAMICS: FROM ADIABATIC TO NONADIABATIC DESCRIPTIONS

Molecular dynamics is a powerful technique for the study of complex systems, where it is largely used to perform statistical sampling over the many degrees of freedom of the system. Within this framework, MD simulations entirely based on MM force fields are commonly used. In light-driven processes however, a QM description of at least part of the system has to be introduced and methods going beyond a ground state description need to be considered in order to follow the irreversible transformation of the initial electronic energy while the system relaxes to a different state or undergoes a photochemical reaction (76).

In principle the time evolution of a given QM system is determined by its time dependent Schrödinger equation, describing both the nuclear ($\boldsymbol{R}$) and electronic ($\boldsymbol{r}$) degrees of freedom

$$i\hbar \frac{\partial}{\partial t} \Psi(\boldsymbol{R}, \boldsymbol{r}, t) = (\hat{\mathcal{H}}_{el}(\boldsymbol{R}, \boldsymbol{r}) + \hat{\mathcal{T}}_{nuc}(\boldsymbol{R})) \Psi(\boldsymbol{R}, \boldsymbol{r}, t). \tag{30}$$

Here, the total Hamiltonian is the sum of the electronic Hamiltonian and the kinetic energy of the nuclei $\hat{\mathcal{T}}_{nuc}$. Solving this problem is challenging and presents a steeply scaling

computational cost, so it is a viable strategy only for small molecules.

To tackle the problem of a large molecular system, possibly interacting with an environment in its full dimensionality, the usual approach consists in considering some sort of classical approximation for the nuclear motions. Within this framework, we necessarily neglect any nuclear quantum effect, such as zero-point energy and tunnelling(77, 78). However, approximate approaches can be introduced to recover at least a part of these effects. For example, in case of the zero point energy a strategy commonly adopted is to perform a sudden heating of the QM region, to approximately recover the energy contribution (79). In case of proton transfers, a successful strategy is to use quantum mechanics to describe just the proton(s) motion (80).

The classical approximation for the nuclear motion can be combined with a Born-Oppenheimer (BO) picture, so that the evolution is fully determined by the potential energy surface of the associated adiabatic electronic state.

Obviously, the BO approximation breaks down when different electronic states get closer in energy, and in that case there can be population transfer between the involved states. Because this phenomenon is often encountered in light driven processes, nonadiabatic dynamics plays a major role in the field.

A large variety of mixed quantum-classical nonadiabatic schemes have been developed (81–83), and among them the most commonly used is the the trajectory-based Surface Hopping (SH) method, pioneered by Tully (84, 85). A trajectory-like approach for the nuclear motion is in fact extremely effective for complex systems as it opens the way to the on-the-fly evaluation of electronic energies and nonadiabatic couplings. More in detail, the reason of the popularity of SH is most probably due to its simplicity, although a careful implementation is needed to obtain meaningful results (86). Surface hopping is a stochastic approach, therefore a simulation consists in a swarm of several trajectories, which is also needed in order to mimic the nuclear quantum wavepacket. In SH the trajectories are independent. This allows to trivially achieve parallel computing, and makes it easy to add trajectories to the swarm, if needed.

Due to its effectiveness in describing light-driven processes in complex systems, here the focus will be mainly on the SH approach. First, the main theoretical and numerical aspects of the general formulation will be presented and discussed, and after that its extension to hybrid QM/C approaches and to multichromophoric systems, will be presented and discussed.

3.1. The Surface Hopping approach

The SH method is a mixed quantum-classical approach in which the nuclear motion is described by a classical trajectory $\boldsymbol{R}(t)$, while the electrons are represented by a wavefunction $\Psi_{el}(\boldsymbol{r}, \boldsymbol{R}, t)$. It is assumed that the equation of motion for the electronic wavefunction is the time dependent electronic Schrödinger equation (TDESE)

$$i\hbar \frac{d\Psi_{el}}{dt} = \hat{\mathcal{H}}_{el}\Psi_{el} \tag{31}$$

where $\hat{\mathcal{H}}_{el}$ is the electronic Hamiltonian, see equation 30. Let $\varphi_k(\boldsymbol{r}; \boldsymbol{R}(t))$ be the eigenstates of $\hat{\mathcal{H}}_{el}$, i.e. the adiabatic states: $\hat{\mathcal{H}}_{el}\varphi_k = E_k\varphi_k$. By expanding the electronic wavefunction in terms of the adiabatic states

$$\Psi_{el}(\boldsymbol{r}, \boldsymbol{R}, t) = \sum_k A_k(t)\varphi_k(\boldsymbol{r}; \boldsymbol{R}(t)) \tag{32}$$

one immediately arrives at the following equation for the coefficients

$$\dot{A}_j = -\frac{i}{\hbar} A_j E_j - \sum_k A_k \dot{\boldsymbol{R}} \cdot \boldsymbol{g}_{jk} \tag{33}$$

where $\boldsymbol{g}_{jk} = \langle \varphi_j | \nabla_{\boldsymbol{R}} | \varphi_k \rangle$ are the nonadiabatic (or derivative) coupling (NAC) vectors. In the above equations 32 and 33, the sums are extended to the number N_{st} of electronic states of interest, which is kept as small as possible to reduce the computational burden.

The TDESE is integrated concurrently with Newton's equation for the nuclei,

$$m_\alpha \frac{\partial^2}{\partial t^2} \boldsymbol{R}_\alpha(t) = -\nabla_\alpha E_k(\boldsymbol{R}(t)) \tag{34}$$

which evolve on the PES E_k of the "current" state k. Actually, at any time during the time evolution the current state may change from k to j, according to a stochastic algorithm, and in that case we have a "hop". The hopping transition probability $T_{k\to j}$ is most often evaluated according to Tully's "fewest switches" scheme. The idea is that $T_{k\to j}$ is larger than zero only if, in the time interval Δt considered, there is a net flux of probability from state k to state j, so that hops are only allowed when actually needed. In particular, the transition probability in the time interval from t to $t + \Delta t$ is (80, 85)

$$T_{k\to j} = \frac{1}{\rho_{kk}} \int_t^{t+\Delta t} \max(0, B_{kj}) dt \qquad \text{with} \quad B_{kj} = 2\Re\left(\rho_{jk} \boldsymbol{g}_{kj} \cdot \dot{\boldsymbol{R}}\right) \tag{35}$$

where $\rho_{kj} = A_k A_j^*$ are the electronic density matrix elements, so that $\rho_{kk} = |A_k(t)|^2$ is the state k probability. Other schemes have been proposed (87, 88), still keeping the concept that the transition probability is obtained from the variation of the state probabilities, rather than from their values, in order to minimize the number of hops. It has been observed (88) that the standard fewest switches algorithm only allows transitions between states which are directly coupled, and therefore cannot account for the "superexchange" mechanism, which refers to a diabatic scheme where a transition between two electronic states $|a\rangle$ and $|b\rangle$ which are not directly coupled is mediated by a state too high in energy to be populated. For example, such a mechanism is important in singlet fission (see below), where a locally excited singlet is converted in a triplet pair, possibly through the coupling with high lying charge transfer states. However, apart from symmetry reasons (which are usually not important in molecular photochemistry), nothing prevents the adiabatic counterparts of $|a\rangle$ and $|b\rangle$ from being coupled: therefore, no special care for superexchange is needed in the fewest switches algorithm when working in the adiabatic representation.

The SH scheme is representation dependent, i.e. the results depend on the electronic basis used to expand Ψ_{el} in equation 32. Here we deliberately restrict ourselves to consider the case in which Ψ_{el} is expanded in terms of adiabatic functions, as SH is known to work best in the adiabatic representation. In fact, the nuclei are expected to follow the adiabatic PES, at least far from strong interaction regions. Moreover, due to the local character of the NAC, hops between adiabatic PES are only likely in regions where the electronic energy differences are small. For SH, this is an important feature, especially considering the rescaling of the nuclear velocities performed after a hop.

On the other hand, the numerical integration of the TDESE is better performed resorting to a diabatic basis. In fact, in contrast to the NAC, the diabatic quantities depend smoothly on the nuclear coordinates and can be easily interpolated in the given numerical

integration timestep Δt. In the local diabatization (LD) method (89), a crude diabatic basis $\{\boldsymbol{\eta}\}$ in the time interval from t to $t+\Delta t$ is defined by setting $\eta_k(\boldsymbol{r}) = \varphi_k(\boldsymbol{r}; \boldsymbol{R}(t))$, for all $k = 1, \dots N_{st}$, i.e. the diabatic states correspond to the adiabatic ones at the beginning of the integration time step (90). The diabatic-to-adiabatic transformation matrix $\mathbf{T}$ at time $t+\Delta t$ is obtained by Löwdin orthonormalization of the overlap matrix $S_{kj} = \langle \varphi_k(t) | \, \varphi_j(t+\Delta t) \rangle$. The derivative couplings in the locally diabatic basis are zero by construction, and the integration of the TDESE only requires the matrix $\mathbf{H} = \left\langle \boldsymbol{\eta} \middle| \hat{\mathcal{H}}_{el} \middle| \boldsymbol{\eta} \right\rangle$, which is in turn obtained from the adiabatic energies. More in detail, $\mathbf{H}(t)$ corresponds to the diagonal matrix $\mathbf{E}(t)$ collecting the adiabatic energies $E_k(t)$, while at time $t+\Delta t$ one has $\mathbf{H}(t+\Delta t) = \mathbf{T}\mathbf{E}(t+\Delta t)\mathbf{T}^{+}$. As mentioned above, at variance with the nonadiabatic couplings, the $\mathbf{H}$ matrix lends itself to a linear interpolation in the time interval Δt, being defined in terms of the constant functions η_k.

In the LD scheme, the risk of missing a strong interaction region or a trivial crossing (i.e. a crossing of two states which are not coupled) is ruled out by construction, thanks to the diabatization procedure. Therefore, the time step for the integration of the TDESE does not need to be smaller than the one for the propagation of the nuclear trajectory (91). At variance, standard methods based on NAC most often require a much smaller time step (83, 87). Moreover, the algorithm employed in the evaluation of the overlap is not influenced by the inclusion of the interaction with an MM environment, polarizable or not. Notice also that the trivial crossing problem is quite commonly encountered, for example in energy or charge transfer in multichromophoric systems, where the strength of the interaction is modulated by the distance between the chromophores. The main drawback with the LD method is the evaluation of the fewest switches transition probability: equation 35 cannot be used, as the NAC are not evaluated (being replaced by the overlaps), and in any case the aim of the LD scheme is precisely to avoid the direct computation of quantities like the integral of equation 35. The expression for the fewest switches transition probability originally proposed in the LD scheme (89), which is still in use nowadays (92, 93), is subject to numerical instabilities, especially in the presence of many weakly interacting states. A better formulation, still in the spirit of the fewest switches algorithm, has been recently proposed by some of us (94).

In many photochemical processes, effects due to the quantum nature of the nuclei, like interference, tunneling, or the zero point energy, can be neglected or circumvented. This is one of the main reasons for the success of independent trajectory methods like SH. However, the quantum decoherence effect, due to the decoupling of two wavepackets traveling on different PES, can seldom be ignored. To understand why quantum decoherence is lost in standard SH, let us start considering the Born Huang expansion for the full quantum wavefunction(95)

$$\Psi(t) = \sum_k |\theta_k(t)\rangle \, \varphi_k \tag{36}$$

where the nuclear wavepackets are represented as generic kets $|\theta_k\rangle$. The full quantum electronic density matrix is then

$$\rho_{kj}^{(q)} = |\theta_k\rangle \, \langle \theta_j| \tag{37}$$

In the coordinates representation, $\rho_{kj}^{(q)}$ is given by the product $\theta_k(\boldsymbol{R},t)\theta_j^*(\boldsymbol{R},t)$. As the two wavepackets evolve on different PES, they will eventually diverge in space. When this happens, one gets $\rho_{kj}^{(q)} \simeq 0$, i.e. zero coherence, so that the motion of the two wavepackets is uncorrelated. The same consideration can be repeated in the momentum ($\boldsymbol{p}$) representation:

two wavepackets located in different regions of the momentum space are decoupled, as the product $\theta_k(\boldsymbol{p},t)\theta_j^*(\boldsymbol{p},t)$ would vanish. Surface hopping behaves very differently in this respect. In fact, in SH the electronic density matrix is $\rho_{kj} = A_k A_j^*$, which may be equal to zero only if one of the two amplitudes is zero, i.e. one of the two states has zero probability. If k is the current state, $A_k \neq 0$ for sure, so that all the other amplitudes A_j are always propagated coherently with the current state, along the nuclear trajectory which evolves on E_k.

In practice, the lack of quantum decoherence can be neglected in SH only for a ultrafast dynamics consisting in a single passage through a strong interaction region. In the other cases, such as multiple passages through a strong interaction region (96, 97), crossing of several strong interaction regions (82), or even for a trajectory wandering for a relatively long time (say, few picoseconds) in a weak coupling region (98), the decoherence effects are, in principle, important. The evaluation of quantum decoherence requires information on the nuclear evolution on the PES different from the current one. This information is clearly not available in independent trajectory methods such as SH, and its computation would be very expensive, especially for large systems, requiring at each time step the evaluation of PES and gradients in several points of the nuclear configurational space. Therefore, a plethora of different approximate algorithms (97–102) for the introduction of decoherence corrections in SH has been developed, all aimed at annihilating, far from strong interaction regions, the amplitudes of the states different from the current one.

3.2. The effects of the environment

Light-driven processes present a strong dependence on the environment. This will be evident especially in Section 4 where the focus will be on excitation energy and electron transfer. There are however, many other processes where the environment not only affects the dynamics but it can also make the whole process unlikely or even not possible.

An example is the excited state proton transfer (ESPT), an important process in both chemical and biological systems. Most of the ESPT processes occur through intermolecular or intramolecular hydrogen bonding, D–H$\cdots$A where the proton donor, D and the proton acceptor, A, are electronegative atoms, such as N or O (103). Upon electronic excitation, the acidity and basicity of donor and acceptor, respectively, are enhanced as a consequence of the redistribution of electronic density in the molecule. In such a way, proton transfer from the donor to the acceptor can take place in the excited state (generally through an ultrafast process) while it is thermodynamically impeded at the ground state. It is clear, that the presence of a protic solvent which interacts through H-bonds with the the acceptor can compete with the proton transfer thus leading to a slower process or even preventing it at all. In addition to that, the environment can change the relative stability of the normal (D–H$\cdots$A) and the tautomeric (D$\cdots$H–A) forms, and affect the energy barrier between them.

The time evolution of the ESPT reaction cannot be obtained from static calculations but it requires an explicit dynamic simulation which in many cases can be performed using an adiabatic approach. Various approaches have been used so far to properly included the effect of the environment in the dynamic description. In some works, classical molecular dynamics was combined with QM/MM potentials based on empirical valence bond (EVB) theory. Many initial configurations and sets of velocities were evolved using classical MD on the excited state EVB potential energy surface, to explore the nonequilibrium response to

photoexcitation for 2-(2-hydroxyphenyl)-4-methyloxazole in solution and in protein (104), and 3-hydroxyflavone in different solvents (105). In particular, in the latter study, it was found that the ultrafast intramolecular proton transfer results from a combination of ballistic transfer and intramolecular vibrational redistribution, which leads to the excitation of a set of low-frequency promoting vibrational modes independently of the solvent. Instead, the analysis of the slow proton transfer trajectories reveals a solvent-mediated proton transfer mechanism, which is limited by diffusion.

Another interesting case of ESPT is that of photoacids which dissociate in the excited state transferring a proton to a nearby solvent molecule or to a strong base present in solution (106–108). In this case the simulation requires to include at least one solvent molecule in the QM subsystem, but in some cases larger clusters are involved. This is the case of reactions in aqueous solutions, where the key role is played by the solvation shells, which facilitate the PT by fluctuations of the hydrogen bond network or breaking and formation of hydrogen bonds. Photoacids have been studied with both adiabatic and adiabatic techniques mostly based on TDDFT eventually combined with electrostatic embedding MM (109, 110).

Another important light-driven process where the environment can dramatically affect the dynamics is singlet fission (SF). In SF a locally excited singlet (or a combination of singlet excitons), here labeled S_1, is converted in a close lying singlet component of a triplet exciton pair (^1TT). As such, it allows to generate two excitons by a single photon. It has been established that charge transfer (CT) states play an important role in the mechanism of singlet fission. According to the energetics, there may be a two-step mechanism, where low-lying CT states are first populated from S_1 before ^1TT is generated. Or else, the transition from the locally excited singlet to ^1TT can be mediated by the interaction with CT states too high in energy to be populated (the superexchange effect). The direct mechanism, in which ^1TT is populated from S_1 without intervention of other states, is also possible. The fundamental role played by CT states in the SF process automatically implies that the environment will have a strong impact on the process through the tuning of the CT energies. Materials most commonly employed in singlet fission are represented by molecular crystals, although covalent dimers are used as well (111). In any case, taking into account correctly the interaction with the environment is of paramount importance, given its strong influence on the SF quantum yield. Several simulations of singlet fission dynamics have been performed, resorting to model Hamiltonians (111, 112), but there are very few fully dimensional SH on-the-fly simulations. Probably one of the main reasons is that the quantum chemistry method used has to be flexible enough to allow at least for a correct treatment of doubly excited configurations and CT states. Prezhdo and co-workers (113) performed a simulation of singlet fission dynamics for pentacene at the interface with C_{60}. Accomasso et al. (114) performed SH simulations of singlet fission in a molecular crystal of 2,5-bis(fluorene-9-ylidene)-2,5-dihydrothiophene, with electronic states obtained using the FOMO-CI method in a semiempirical framework. The simulation was brought about in a QM/MM scheme, inserting two or three molecules in the QM part. Difference in the energetics of locally excited, CT and ^1TT states were found to be more important than the changes in the couplings between these states, confirming the importance of a correct assessment of the influence of the environment on the electronic energies.

From this brief introduction it is clear that the inclusion of the environment effects in the adiabatic or nonadiabatic modeling of light-driven processes is necessary to achieve a realistic picture. Such a modeling, however, requires to carefully consider some new issues

with respect to an isolated molecular system. Still limiting our analysis to hybrid methods using a classical embedding, the following specificities have to be taken into account: i) the environment modifies the energies and forces acting on the QM atoms, ii) in case of an atomistic model there are additional degrees of freedom that have to be propagated along the dynamics as well, and iii) in case of nonadiabatic dynamics such as SH, a polarizable embedding introduces additional complexity in the description of multiple excited states.

If the selected model is a QM/MM with an electrostatic embedding, all these issues are easily solved. Within this framework, in fact, the atoms of the environment are described by fixed point charges which behave classically. As a result, their presence only increases the number of coordinates to be treated in the classical equation of motion. Moreover, the additional electrostatic contribution to the forces acting on the QM subsystem can be obtained exactly in the same way one calculates the effects of the nuclei. Once taken into account these two aspects, both NAD or BO simulations described so far can be performed with only a limited increase of the computational cost.

On the contrary, the use of a polarizable QM/classical formulation introduces new theoretical and numerical issues that have to be carefully considered. In the context of dynamics, atomistic approaches are by far preferable to continuum ones. Continuum models in fact are not easy to be recast in a time-dependent formulation. So far, the most effective in this direction are the ones based on real-time (RT) descriptions. This framework has been explored within a RT-TDDFT formulation by introducing an equation of motion for the ASC (115, 116). This is achieved by rewriting eq. 2 in the frequency domain and using the full spectrum of the solvent frequency-dependent dielectric permittivity. By Fourier transforming the resulting equation back to the time domain, one arrives at the definition of time-dependent ASCs to be used in combination with the quantum Liouville equation, which describes the time evolution of the electronic degrees of freedom. Such a combination leads to working equations for the QM density propagation in the presence of an environment that rigorously account for the delayed polarization (nonequilibrium effects). RT-TDDFT approaches have been also combined with polarizable embedding QM/MM using an induced dipole formulation (117, 118). However, these approaches are mostly focused on the description of the time evolution of the electronic density following a perturbation and as such they are generally used for simulating spectroscopy. On the contrary, their extension to include nuclear dynamics is neither straightforward nor computationally effective.

When compared to continuum models, polarizable atomistic approaches are clearly a much better strategy to include environment effects in both adiabatic and nonadiabatic dynamics. For adiabatic approaches, the inclusion of a polarizable embedding can be obtained by using the formulations of both energy and gradients presented in Section 2.3. As a matter of fact, ground state BOMD in combination with a polarizable embedding QM/MM has been already presented in the literature both using a Drude (119) or an induced dipole formulation (37, 42, 120). Moreover, a very recent extension to excited state dynamics within a TDDFT approach has been presented still using the induced dipole formulation (71).

In a nonadiabatic framework, instead, the inclusion of polarization in the the classical environment is much more problematic. In fact, each electronic state of the QM system polarizes the classical part in a different way, and is then characterized by a different $\hat{\mathcal{H}}_{el}$. This results in an incorrect description of the PES in the vicinity of avoided crossings and conical intersections.

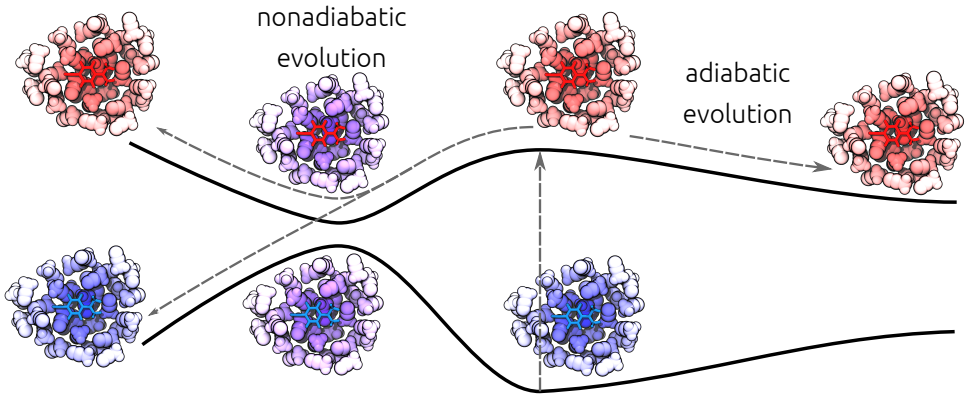

Figure 2

Schematic representation of two possible relaxation processes of an excited molecule embedded in a polarizable environment. The two electronic states of the QM molecule are depicted in blue (GS) and red (S1), the response of the environment is colored accordingly. In the case depicted to the right, upon excitation the molecule undergoes an adiabatic relaxation process which involves only the S1 state, since the GS is far in energy. The environment will always respond to the S1 density. In the case depicted to the left, the molecule goes through a region of strong nonadiabatic coupling with the ground state, so the relaxation involves both the states. The environment response is a average over the two states (purple) in the region of strong NAC, whereas is specific of the state elsewhere.

These conceptual difficulties have not found an effective solution so far, and, to the best of our knowledge, no trajectory-based nonadiabatic simulations with polarizable MM environment have been reported in the literature. Despite that, here we can try to sketch two possible approximations which could be used as a starting point for a future implementation. The first one is to introduce a LR description, which, as discussed in the previous Section, does not involve a state-specific response of the environment. The drawbacks of this formulation have been already discussed in the previous section and involve limitations both in the choice of the QM method (that is generally limited to single reference approaches) and in the environment response which does not account for the state-specific relaxation of the polarization. The second strategy is that of employing a state-averaged polarization in the vicinity of crossings and a state specific approach elsewhere. Hagras and Glover proposed an algorithm to interpolate between the two descriptions, in terms of a switching function depending on the energy difference between a reference state and the other electronic states considered (121). A schematic representation of the second strategy is shown in Fig. 2. This strategy, contrary to the first, has the advantage of being the most natural for multireference QM approaches, such as CASSCF, which are often required in nonadiabatic simulations.

3.3. Multichromophoric systems

Many fundamental light-driven processes are not localized on a single molecule but they involve (large) multichromophoric aggregates. The processes involved in light-harvesting in natural and artificial systems, such as charge and energy transfer, are well known examples. While SH and other NAD approaches can still be applied, some changes have to be included

with respect to their standard formulation.

The first one concerns the feasibility of these approaches in the presence of molecular aggregates. Due to the rapid increase in the computational cost with the size of the aggregate, approximate approaches have been devised and successfully used. Among them, one of the most commonly adopted is the Frenkel exciton model (122–124). Within this framework, it is assumed that the electronic states of the aggregate can be represented as linear combinations of diabatic states, namely excitations localized on each individual chromophore. Taking into account only one state per chromophore (or "site") for simplicity, the electronic Hamiltonian of an aggregate of M sites becomes

$$\hat{\mathcal{H}}_{el} = |g\rangle \, \mathcal{E}_g \, \langle g| + \sum_{J}^{M} |J\rangle \, \mathcal{E}_J \, \langle J| + \sum_{I \neq J}^{M} |I\rangle \, V_{IJ} \, \langle J| \tag{38}$$

where $|g\rangle$ is the ground state and $|J\rangle$ is a locally excited state on the J-th chromophore. In turn, $|J\rangle$ is expressed as an antisymmetrized product of monomer wave functions

$$|J\rangle = \varphi_1^{(g)} \wedge \varphi_2^{(g)} \wedge \ldots \wedge \varphi_J^{(ex)} \wedge \ldots \wedge \varphi_M^{(g)} \tag{39}$$

and similarly for the ground state $|g\rangle$. The individual chromophores wavefunctions, together with the site energies $\mathcal{E}_J$, are obtained by quantum chemistry calculations on single sites. An advantage of this quasi-diabatic scheme is the possibility of introducing ad-hoc corrections to the site energies. In a semiempirical framework, the individual chromophore wavefunctions are automatically orthogonal, and this "strong orthogonality" condition is normally also assumed in the ab initio case, so that $\langle I| \, J\rangle = \delta_{IJ}$.

The excitonic coupling V_{IJ} is well approximated by the Coulomb integral of the transition charge densities for sites I and J:

$$V_{IJ} \simeq V_{Coul} = \int \mathrm{d}\mathbf{r}_1 \mathrm{d}\mathbf{r}_2 \frac{\rho_I^{\mathrm{tr}}(\mathbf{r}_1) \, \rho_J^{\mathrm{tr}}(\mathbf{r}_2)}{r_{12}} \tag{40}$$

where $\rho_{I/J}^{\mathrm{tr}}(\mathbf{r})$ are the transition densities of the donor and acceptor, respectively.

The presence of an environment has two major effects on the couplings. First, a system polarized by the environment has different electronic properties, and thus a different transition density. Second, the environment can screen the Coulomb interaction between the transition densities, so that the coupling is mediated by the environment itself. For a homogeneous environment it can be thought as a dielectric screening of the Coulomb coupling and roughly scales the total Coulomb coupling by the squared refraction index of the medium. However, even in homogeneous media, this term strongly depends on the relative orientations of the donor and acceptor transition moments (125), and in heterogeneous media it also depends on the nature and the orientation of the molecules of the environment (126). Excitonic couplings will be further discussed in Section 4 in relation with model Hamiltonian approaches.

For a modeling point of view, the first effect is easily introduced with any multiscale strategy capable of polarizing the electronic density. However, only a polarizable model is able to capture the second effect, as it indeed arises from the polarizable nature of the environment (34, 125, 127). This term is related to the response equation 24 and, in the same formalism, can be written as

$$V_{env} = \langle X[\rho_I^{\mathrm{tr}}], \Psi(\rho_J^{\mathrm{tr}}) \rangle \tag{41}$$

where $\Psi(\rho_I^{\mathrm{tr}})$ is the electrostatic property generated by the I transition density ρ_I^{tr}, and $X[\rho_I^{\mathrm{tr}}]$ is the polarization induced by the J transition density. Given the bilinear form of the interaction, the coupling term does not change by exchanging the I and J labels.

In SH implementations, the Coulomb integral has been evaluated by approximating each transition density with a site-centered dipole (122), or with atomic charges (123). In the TrEsp method (128), these charges are computed by fitting the electrostatic potential generated by the transition density, in the same way as ESP charges. Employing a method allowing to obtain atomic charges depending as little as possible on the molecular geometry (129) could be beneficial in this context, especially considering that the gradient of the excitonic coupling is usually obtained neglecting the dependence of these charges on nuclear coordinates.

The diagonalization of the electronic Hamiltonian of equation 38 yields the adiabatic ground $\varphi_0 = |g\rangle$ and excited states $\varphi_i = \sum_J c_{J,i} |J\rangle$, on which the SH dynamics is performed. The corresponding nonadiabatic couplings $\boldsymbol{g}_{ij}$ have been approximated by Martìnez and coworkers(122) resorting to the Hellmann-Feynman theorem

$$\boldsymbol{g}_{ij} \simeq \frac{\mathbf{c}_i^+ \nabla_{\boldsymbol{R}} \mathbf{H}\, \mathbf{c}_j}{E_j - E_i} \tag{42}$$

where $\mathbf{H}$ is the electronic Hamiltonian matrix in the excitonic basis. In this way, the calculation of NAC does not increase the computational burden, but intra-chromophore couplings are neglected, so that the decay to the ground state is not taken into account (for example, an isolated chromophore would never decay).

On the other hand, when the local diabatization method presented in Section 3.1 was adopted (123), the evaluation of the overlaps $S_{ij} = \langle \varphi_i(t) |\, \varphi_j(t + \Delta t)\rangle$ was performed without introducing further approximations, with a procedure conceptually simple but more computationally expensive. In fact, the S_{ij} are readily obtained in terms of the excitonic overlaps $S_{IJ} = \langle I(t) |\, J(t + \Delta t)\rangle$ using the coefficients $c_{J,i}$. In turn, from equation 39 and exploiting the orthogonality of individual chromophore wavefunctions, S_{IJ} is just a product of single-site overlaps

$$\begin{aligned} S_{IJ} = &\left\langle \varphi_1^{(g)}(t) \middle|\, \varphi_1^{(g)}(t + \Delta t) \right\rangle \ldots \left\langle \varphi_I^{(ex)}(t) \middle|\, \varphi_I^{(g)}(t + \Delta t) \right\rangle \ldots \\ &\left\langle \varphi_J^{(g)}(t) \middle|\, \varphi_J^{(ex)}(t + \Delta t) \right\rangle \ldots \left\langle \varphi_M^{(g)}(t) \middle|\, \varphi_M^{(g)}(t + \Delta t) \right\rangle . \end{aligned} \tag{43}$$

Overlaps involving the excitonic ground state $|g\rangle$ are obtained in the same way, and this allows to describe correctly the decay to S_0.

Taking into account the strong orthogonality assumption, and the approximation involved in the evaluation of the excitonic couplings V_{IJ}, the Frenkel exciton model is better suited to treat assemblies in which there is not a significant overlap between the single chromophore wavefunctions.

A similar formulation can also be used in the context of charge transfers. for example, to simulate charge transport in organic semiconductors, Blumberger and coworkers have developed the fragment orbital-based SH (FOB-SH) method (130, 131), which is based on a one-particle approximation of the electronic wavefunction. In particular, a non-orthogonal basis set, which plays the same role as the exciton basis in the Frenkel exciton model, is built using the LUMO orbitals of the individual isolated sites. The site energies are approximated by a classical force field, while the coupling between sites V_{IJ} is taken as directly proportional to the overlap between the site-localized orbitals. This method represents a

very cost effective way to describe realistically charge transport in molecular assemblies. However the introduction of the interaction with the environment in the site-localized basis is expected to increase considerably the computational burden.

4. MODEL HAMILTONIAN APPROACHES

In the previous Section we have shown how to obtain a description of photoinduced dynamics taking explicitly into account the system and environment's nuclear coordinates, albeit at the price of a classical description of their motion. A different, and in certain ways opposite, path can be taken, by projecting all of the complexity of the system into an effective Hamiltonian, which models the electronic and vibronic interactions within the total system, but retaining the quantum nature of the nuclei. Such a strategy is useful when describing multichromophoric processes, such as charge and energy transfer.

In many energy and electron transfer processes, the initial and final states are strongly localized and can be treated as quasi-diabatic(132), forming thus a useful starting point for studying inter-chromophoric processes. Within this framework, we can write the total Hamiltonian as

$$\hat{\mathcal{H}} = \hat{\mathcal{H}}_{el} + \hat{\mathcal{H}}_{vib} + \hat{\mathcal{H}}_{el-vib} \tag{44}$$

where $\hat{\mathcal{H}}_{el}$ is the electronic Hamiltonian in a quasi-diabatic basis of electronic states, such as the one described in eq. 38 of the previous section. For simplicity, here we assume that there exist two electronic states i (initial) and f (final) that are relevant to the photoinduced interchromophoric process.

The vibrational part of the Hamiltonian comprises all the nuclear degrees of freedom of the molecules involved in the photoinduced processes and of the environment. These degrees of freedom are usually approximated as a manifold of harmonic oscillators linearly coupled to the electronic states, in the displaced harmonic oscillator model (See Figure 3)

$$\hat{\mathcal{H}}_{el-vib} = \sum_k \omega_k \sqrt{\hbar\omega_k}\hat{x}_k \left(g_k^i \left|i\right\rangle \left\langle i\right| + g_k^f \left|f\right\rangle \left\langle f\right| \right) \tag{45}$$

$$\hat{\mathcal{H}}_{vib} = \sum_k \frac{\omega_k^2}{2}(\hat{x}_k^2 + \hat{p}_k^2). \tag{46}$$

Here, the index k runs over the normal modes, and $\hat{x}_k$ and $\hat{p}_k$ are the mass-weighted position and momentum operator associated with the k-th mode with frequency ω_k. The quantities $g_k^{i/f}$ define the dimensionless coupling between mode k and state i/f (Figure 3a). The dimensionless displacement between the minima of states i and f are described by the Huang-Rhys factors

$$S_k^{if} = \frac{1}{2}\left(g_k^i - g_k^f\right)^2. \tag{47}$$

Passing from the i minimum to the f minimum, the f energy decreases by a quantity λ called the reorganization energy. In this model, the reorganization energy is the same for the $i \to f$ and $f \to i$ transitions, and

$$\lambda = \sum_k \lambda_k = \sum_k \hbar\omega_k S_k^{if}. \tag{48}$$

When the discrete normal modes are replaced with a continuum, a spectral density $J(\omega)$ can be defined as (133, 134)

$$J(\omega) = \pi \sum_k \delta(\omega - \omega_k)\omega_k^2 S_k^{if}. \tag{49}$$

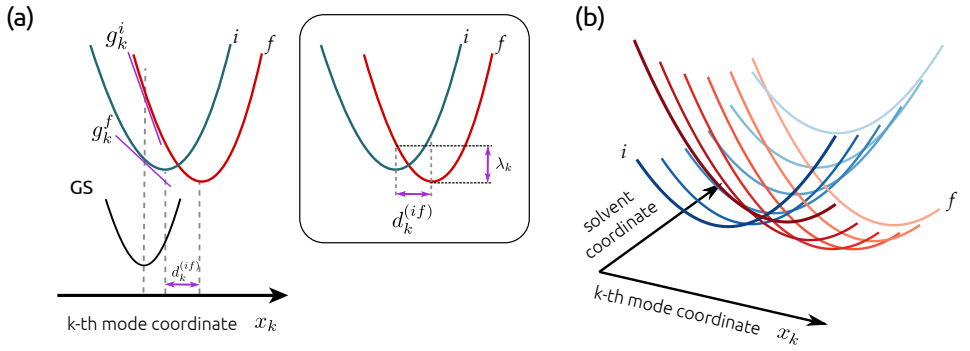

Figure 3

(a) Depiction of the displaced harmonic oscillator comprising the ground state and states i and f along the k-th normal mode. In the box, the displacement between the minima $d_k^{(if)}$ and the corresponding reorganization energy $\lambda_k = \hbar S_k \omega_k$ are shown. (b) Initial- and final-state PESs along two modes, one normal mode of the chromophore(s) and one of the solvent. Several slices along the chromophore normal modes are shown at different values of the solvent coordinate.

The spectral density can be also derived from linear-response theory (135, 136), which offers a way to map any motion of the environment to an effective collection of harmonic modes.

In general, it is useful to separate the internal vibrations of the photo-active moieties from the motions of the surrounding environment, i.e. $J(\omega) = J_{\text{int}}(\omega) + J_{\text{env}}(\omega)$. Likewise, the reorganization energy can be separated as $\lambda = \lambda_{\text{int}} + \lambda_{\text{env}}$.

This framework allows for the description of different photoinduced processes in several classes of systems. Furthermore, the ingredients of this Hamiltonian, such as site energies, electronic couplings, and vibronic couplings, can be easily obtained from (multiscale) quantum chemical calculations. The power of these approaches is their simplicity, coupled to the easy physical interpretation of the effective Hamiltonians.

Model Hamiltonian approaches can be classified according to the relative strengths of the electronic (V) and the vibronic couplings (λ). In particular, when $V \ll \lambda$, the so-called "weak coupling limit" applies, and the dynamics can be described with a system of kinetic equations obtained from a perturbative approach as discussed in the following section. We recall, however, that in many cases the two couplings have comparable magnitudes or that the electronic coupling is much larger than the vibronic one. These are the most common regimes observed, for example, in the pigment-protein complexes used by photosynthetic organisms to collect sunlight. In these cases, advanced levels of quantum dynamics theories and computational approaches become necessary as simple perturbation theories cannot be applied (137, 138).

4.1. Weak coupling limit

In the weak coupling limit, the dynamics of the system can be described with a Golden Rule perturbative treatment of V (139–141), that is, the rate of transfer between an initial i and a final f state can be calculated from the electronic coupling V_{if} as:

$$k_{if} = \frac{2\pi}{\hbar} |V_{if}|^2 \sum_{v,v'} p(E_v) \left|\langle v|v'\rangle\right|^2 \delta(E_{iv} - E_{fv'}) = \frac{2\pi}{\hbar} |V_{if}|^2 \,\text{FCWD} \qquad (50)$$

Here, the indices v and v' run over the vibrational states of i and f, and $p(E_v)$ is the equilibrium population of the initial state. The sum is also denoted as the FCWD factor (Franck-Condon weighted density of states). Two other major assumptions are made in this case: the vibrational degrees of freedom are completely equilibrated, hence the $p(E_v)$ factor, and that the electronic coupling does not depend on the nuclear coordinates, which corresponds to the Condon approximation. Assuming equilibration, the Golden Rule rates obey the detailed balance condition, i.e. $\frac{k_{if}}{k_{fi}} = \exp(-\beta\hbar\omega_{if}^{(0)})$, where $\hbar\omega_{if}^{(0)}$ is the adiabatic energy difference between initial and final states.

Making use of the properties of the Fourier transform, the Golden Rule equation 50 can be recast as a time-domain integral (142)

$$k_{if} = \frac{|V_{if}|^2}{\hbar^2} \int_{-\infty}^{\infty} \mathrm{d}t\, e^{i\omega_{if}^{(i)}t - g_{if}(t)} \tag{51}$$

where $\hbar\omega_{if}^{(i)}$ is the energy difference between the two states i and f calculated at the i equilibrium geometry, and $g_{if}(t)$ is the cumulant generating function, which in the linear vibronic coupling approximation can be written as (132, 142–144):

$$g_{if}(t) = -\sum_k \left(S_k^{if} \left[(\bar{n}_k + 1)(e^{-i\omega_k t} - 1) + \bar{n}_k (e^{+i\omega_k t} - 1) \right] - i S_k^{if} \omega_k t \right) \tag{52}$$

Here, the Huang-Rhys factors S_k^{if} (eq. 47) describe how the $i-f$ energy gap couples to the normal mode k, and $\bar{n}_k$ is the average vibrational quantum number of oscillator k according to the Bose-Einstein distribution. A more general expression for $g_{if}(t)$ can be obtained, taking into account the mixing of normal modes passing from state i to state f, also called Duschinsky rotations (141). The function $g_{if}(t)$ can be written in terms of the the spectral density defined above (135, 145, 146).

These expressions are completely general, and, although they have mainly been developed with relation to charge transfer processes (144), they make no specification on the nature of initial and final states. In the following, we will consider the specificity of each type of photoinduced process in order to find the simplest expressions for the FCWD factors and the strategies used to compute the electronic couplings.

4.2. Excitation Energy Transfer

In excitation energy transfer (EET), the initial state is an excited state localized on a *donor* (part of) molecule, and the final state is localized on an *acceptor* moiety. EET can occur between singlet states or between a singlet and a triplet. In the latter case, the process is known as triplet energy transfer (TET) or Dexter energy transfer.

In general, the electronic coupling involved in EET can be written as $V_{Coul} + V_{short}$, where V_{Coul} is the Coulomb coupling shown in eq. 40, and V_{short} is a term containing all short-range contributions (147, 148). The Coulomb coupling is the dominant term in singlet EET. When the donor and acceptor moieties are well separated, the leading term in the multipole expansion of V_{Coul} gives rise to the well known dipolar coupling of Förster theory, and to the r^{-3} dependence of the EET coupling (and the r^{-6} dependence of the EET rate).

The Coulomb coupling and its approximations have been discussed in Section 3.3. Here, we remark that the ingredients of eq. 40, namely the transition densities, are easily accessible from electronic structure calculations on the separate donor and acceptor, and several methods have been devised to practically compute these quantities (34, 127, 128).

In singlet energy transfer, the short-range terms become important when the electron densities of the donor and acceptor moieties overlap, and when the two moieties are covalently linked. The Coulomb contribution to the coupling is identically zero in triplet energy transfer, and therefore this process only occurs when there is overlap between the electron densities of the interacting moieties.

While it is possible to evaluate the short-range terms from calculations on the separate molecules, a much more accurate approach starts from a "supermolecule" calculation containing both the donor and the acceptor, followed by a diabatization scheme to recover the localized states, which will be, by construction, orthogonal and localized as much as possible onto the donor or acceptor fragments, respectively.

Among the diabatization methods, the Fragment Excitation Difference (FED) scheme was specifically designed to localize valence excited states on molecular fragments defined by the investigator (149, 150). The FED scheme finds the combination of (adiabatic) excited states that localizes as much as possible the excitation density $\rho^{ex}_{mn}(r)$, namely the sum of attachment and detachment densities (149). The localized states can be found by diagonalizing the matrix

$$\Delta x_{mn} = \int_{r\in D} \rho^{ex}_{mn}(r)\,\mathrm{d}\mathbf{r} - \int_{r\in A} \rho^{ex}_{mn}(r)\,\mathrm{d}\mathbf{r} \tag{53}$$

Diabatization methods like the FED scheme are called "additional operator" diabatizations. This additional operator, such as Δx in FED, is defined in order to have maximal/minimal eigenvalues for the localized states. Transforming the electronic Hamiltonian matrix (which is diagonal in the adiabatic basis) in the basis of Δx eigenvectors yields a matrix whose off-diagonal elements represent the electronic couplings (148). This scheme can be generalized easily to triplet states, where the spin density $\sigma(\mathbf{r})$ is localized on the fragments (151).

In addition to the coupling, the other fundamental term to evaluate to get the EET rate is the FCWD factor. The calculation of this quantity can be simplified by assuming that valence excited states localized on one molecule are essentially coupled only to vibrations of the same molecule. The normal modes can then be partitioned in those of the donor and of the acceptor. It is then easy to see that in this case the FCWD factor from eq. 50 reduces to

$$\mathrm{FCWD} = \int_{-\infty}^{\infty} \mathrm{d}E f_D(E) f_A(E) \tag{54}$$

where $f_D(E)$ and $f_A(E)$ are the FCWD functions of the donor and acceptor, respectively, and are readily derived from the donor emission and acceptor absorption spectra (147, 148). For this reason, the FCWD factor is also called *spectral overlap* when considering EET processes.

The environment influences the EET rate in different ways through the electronic coupling and the FCWD factor. Clearly, the FCWD factor depends on the energies of the donor- and acceptor-localized excited states, which in turn are tuned by the surrounding environment. This effect is particularly important in pigment-protein complexes, where both the rate and overall direction of EET are determined by how the protein tunes the pigments' excitation energies. Another important (and often overlooked) effect is the explicit polarization term which we discussed in Section 3.3. This term can reduce the EET rate by a factor of four, depending on the specific system and orientation between the chromophores (147).

Several works employed the theory described here to compute EET rates in artificial model dyads in solution. The relatively limited computational requirements make this approach amenable to high-throughput analyses of donor-acceptor dyads (152). By coupling calculations in solution with a continuum model, it is possible to rationalize the solvent-dependent behaviour of EET rates and to assign different timescales observed in transient absorption to different conformers (153). In an analogous way, Curutchet et al. (126) showed how the EET rate in a photosynthetic pigment-protein complex can be tuned by the heterogeneous protein environment.

4.3. Photoinduced Electron Transfer

In photoinduced electron transfer, the initial state is usually a locally excited state, directly generated by light absorption, whereas the final state is a charge-separated state, where the initially excited moiety remains either positively charged after donating an electron, or negatively charged after donating a hole. In the latter case, the process is also called "hole transfer" (HT).

The electronic couplings involved in ground-state electron and hole transfer can be expressed on the basis of frozen molecular orbitals of the donor and acceptor molecule (154). For example, the hole transfer coupling is related to the matrix element of the Fock operator between the frozen HOMO orbitals of the two molecules

$$V_{DA} \sim \langle \phi_D^{HOMO} | \hat{F} | \phi_A^{HOMO} \rangle \tag{55}$$

similarly, the electron transfer coupling is related to the Fock matrix element between the LUMO orbitals of the two molecules. In principle, also photoinduced ET/HT couplings may be approximated by directly calculating the orbitals of the isolated molecules, and then computing the relevant matrix elements (155), but this procedure is less accurate for photoinduced ET/HT than for the corresponding ground-state processes (150).

As in the case of the EET coupling, the couplings involved in photoinduced ET/HT can be obtained from a diabatization scheme with an additional operator. The fragment charge difference scheme (FCD), originally proposed by Voityuk and Rosch for groud-state ET (156), was later generalized to the photoinduced case (157). In FCD, the additional operator is defined by its matrix elements Δq_{mn}

$$\Delta q_{mn} = \int_{r \in D} \rho_{mn}(r)\, \mathrm{d}\mathbf{r} - \int_{r \in A} \rho_{mn}(r)\, \mathrm{d}\mathbf{r} \tag{56}$$

where $\rho_{mn}(r)$ is the transition density between states m and n, and the state density when $m = n$. Similarly to the FED scheme, here the transformation to diabatic states can be obtained by diagonalizing a two-by-two matrix of Δq values. However, it was shown that, for couplings involving charge-separated states, more than two adiabatic states should be considered as a basis to construct localized states (157, 158). This led to generalizing FCD to a multistate treatment (158), where a $N \times N$ Δq matrix is diagonalized to separate three subspaces, characterized by local excitations ($\Delta q = 0$) and by pure charge-transfer excitations ($\Delta q = 1$ or -1). Within each subspace, the states are additionally rotated in order to ensure that the subspace Hamiltonian is diagonal. For couplings between covalently bonded moieties, the multistate treatment has shown that several adiabatic excited states are needed to recover a localized charge-transfer state (158). Multistate FCD additionally allows for an automation of the coupling calculation (158).

The theory detailed in Section 4.1 can be readily applied to photoinduced ET/HT processes; however, it requires a computational evaluation of the harmonic frequencies and Huang-Rhys factors used in eq. 52. Within the linear vibronic coupling approximation, only ground-state normal mode frequencies are needed, and Huang-Rhys factors can be computed from the displacement in equilibrium positions between the different states (142).

The popular Marcus theory and its variations (146, 159) might be viewed as precise approximations to the Golden Rule rate theory (142). In particular, by two key approximations, the high-temperature and the short-time limits, eq. 51 can be transformed into the classical Marcus equation:

$$k_{if} = \frac{|V_{if}|^2}{\hbar}\sqrt{\frac{\pi}{\lambda k_B T}}\exp\left(-\frac{(\Delta G^\circ + \lambda)^2}{4\lambda k_B T}\right) \tag{57}$$

where ΔG° is the free energy difference between the initial and final state. These assumptions are valid when the reorganization energy is mainly due to the environment, i.e. $\lambda_{env} \gg \lambda_{int}$.

The importance of the environment in tuning photoinduced ET can be understood from the involvement of a charge-separated state, which is strongly influenced by the electrostatics of the surroundings, much more than locally excited states. In addition, a polar environment gives a large contribution to the reorganization energy, as the environment polarization changes significantly between the locally excited initial state and the charge-separated final state. Originally, Marcus derived an expression for the solvent contribution to the reorganization energies, approximating the donor and acceptor moieties as spheres in a continuum dielectric. Within this model, $\lambda_{env} \propto \left(\frac{1}{\varepsilon_{op}} - \frac{1}{\varepsilon_{st}}\right)$, where ε_{op} and ε_{st} are the optical and static dielectric constants of the medium.

Any modern CSM can be directly applied to calculating reorganization energies and free energy differences, by exploiting the difference between nonequilibrium and equilibrium solvation (160, 161), in a more refined analogue of the simplified Marcus model. Similarly, MD-based techniques can be used to determine reorganization energies in the linear response approximation (144, 162).

The photoinduced ET rates computed with the formalism here described have been used to understand the photoprotective chlorophyll quenching in pigment-protein complexes, and how it can be tuned by the protein environment (163). By analyzing the solvent-dependence of the electronic energies and couplings, Stasyuk et al. found that the photoinduced ET pathways strongly depend on solvent polarity in a molecular triad (164). Finally, combinations of photoinduced ET and EET calculations were used to obtain a complete understanding of the photophysics of molecular dyads (161, 165). Inserting the calculated rates in a kinetic model allowed for the time-resolved description of electronic populations (161).

5. Conclusions

The modeling of light-driven processes has seen an enormous development in the last decades both in terms of realism and accuracy. Part of these achievements can surely be connected to the introduction of multiscale approaches which combine quantum chemical methods with classical models. It is in fact thanks to this hybrid strategy that the quantum chemical methods developed to study the photophysics and the photochemistry of small isolated molecules have been generalized to describe complex systems such as proteins and DNA, on one side, and interfaces and materials, on the other side. In this review, we have presented

the most recent advances of this strategy and discussed methodological and physical aspects of its application to selected light-driven processes. From this analysis, what should clearly come out is that the hybrid strategy is now a mature approach which can be successfully integrated with the most powerful experimental techniques so to obtain a complete and accurate picture of light-matter interaction in complex systems. Some aspects can still be improved but the infrastructure of the strategy is robust and its future is certainly bright especially if an effective combination with machine learning methods will be realized. Some examples in this direction have already appeared, for example in the construction of force fields or in providing potential energy surfaces and forces to be used in nonadiabatic dynamics (166, 167), but many more will come in the near future.

DISCLOSURE STATEMENT

The authors are not aware of any affiliations, memberships, funding, or financial holdings that might be perceived as affecting the objectivity of this review.

ACKNOWLEDGMENTS

L.C. and B.M. acknowledge funding by the European Research Council, under the grant ERC-AdG-786714 (LIFETimeS).

LITERATURE CITED

1. Warshel A, Levitt M. 1976. Theoretical studies of enzymic reactions: dielectric, electrostatic and steric stabilization of the carbonium ion in the reaction of lysozyme. *J. Mol. Biol.* 103:227–249
2. Rivail JL, Rinaldi D. 1976. A quantum chemical approach to dielectric solvent effects in molecular liquids. *Chem. Phys.* 18:233–242
3. Miertuš S, Scrocco E, Tomasi J. 1981. Electrostatic interaction of a solute with a continuum. A direct utilizaion of AB initio molecular potentials for the prevision of solvent effects. *Chem. Phys.* 55:117–129
4. Cramer, CJ and Truhlar, DG. 1999. Implicit solvation models: Equilibria, structure, spectra, and dynamics. *Chem. Rev.* 99:2161–2200
5. Orozco M, Luque FJ. 2000. Theoretical Methods for the Description of the Solvent Effect in Biomolecular Systems. *Chem. Rev.* 100:4187–4226
6. Tomasi J, Mennucci B, Cammi R. 2005. Quantum Mechanical Continuum Solvation Models. *Chem. Rev.* 105:2999–3093
7. Klamt A. 2011. The COSMO and COSMO-RS solvation models. *Wiley Interdiscip. Rev.: Comput. Mol. Sci.* 1:699
8. Gao J. 1996. Hybrid Quantum and Molecular Mechanical Simulations: An Alternative Avenue to Solvent Effects in Organic Chemistry. *Acc. Chem. Res.* 29:298–305
9. Lin H, Truhlar DG. 2006. QM/MM: what have we learned, where are we, and where do we go from here? *Theor. Chem. Acc.* 117:185–199
10. Senn HM, Thiel W. 2009. QM/MM methods for biomolecular systems. *Angew. Chem. Int. Ed.* 48:1198–1229
11. van der Kamp MW, Mulholland AJ. 2013. Combined Quantum Mechanics/Molecular Mechanics (QM/MM) Methods in Computational Enzymology. *Biochemistry* 52:2708–2728
12. Halgren TA, Damm W. 2001. Polarizable force fields. *Curr. Opin. Struct. Biol.* 11:236–242

13. Warshel A, Kato M, Pisliakov AV. 2007. Polarizable force fields: history, test cases, and prospects. *J. Chem. Theory Comput.* 3:2034–2045
14. Cieplak P, Dupradeau FY, Duan Y, Wang J. 2009. Polarization effects in molecular mechanical force fields. *J. Phys.: Condens. Matter* 21:333102–22
15. Luque FJ, Dehez F, Chipot C, Orozco M. 2011. Polarization effects in molecular interactions. *Wiley Interdiscip. Rev.: Comput. Mol. Sci.* 1:844–854
16. Jing Z, Liu C, Cheng SY, Qi R, Walker BD, et al. 2019. Polarizable Force Fields for Biomolecular Simulations: Recent Advances and Applications. *Annu. Rev. Biophys.* 48:371–394
17. Nerenberg PS, Head-Gordon T. 2018. New developments in force fields for biomolecular simulations. *Curr. Opin. Struct. Biol.* 49:129–138
18. Inakollu VS, Geerke DP, Rowley CN, Yu H. 2020. Polarisable force fields: what do they add in biomolecular simulations? *Curr. Opin. Struct. Biol.* 61:182–190
19. Bondanza M, Nottoli M, Cupellini L, Lipparini F, Mennucci B. 2020. Polarizable embedding QM/MM: the future gold standard for complex (bio)systems? *Phys. Chem. Chem. Phys.* 22:14433–14448
20. Gordon MS, Freitag MA, Bandyopadhyay P, Jensen JH, Kairys V, Stevens WJ. 2001. The Effective Fragment Potential Method: A QM-Based MM Approach to Modeling Environmental Effects in Chemistry. *J. Phys. Chem. A* 105:293–307
21. DeFusco A, Minezawa N, Slipchenko LV, Zahariev F, Gordon MS. 2011. Modeling Solvent Effects on Electronic Excited States. *J. Phys. Chem. Lett.* 2:2184–2192
22. Gurunathan PK, Acharya A, Ghosh D, Kosenkov D, Kaliman I, et al. 2016. Extension of the Effective Fragment Potential Method to Macromolecules. *J. Phys. Chem. B* 120:6562–6574
23. Xie W, Gao J. 2007. The Design of a Next Generation Force Field: The X-POL Potential. *J. Chem. Theory Comput.* 3:1890–1900
24. Xie W, Orozco M, Truhlar DG, Gao J. 2009. X-Pol Potential: An Electronic Structure-Based Force Field for Molecular Dynamics Simulation of a Solvated Protein in Water. *J. Chem. Theory Comput.* 5:459–467
25. Brunk E, Rothlisberger U. 2015. Mixed Quantum Mechanical/Molecular Mechanical Molecular Dynamics Simulations of Biological Systems in Ground and Electronically Excited States. *Chem. Rev.* 115:6217–6263
26. Curutchet C, Mennucci B. 2017. Quantum Chemical Studies of Light Harvesting. *Chem. Rev.* 117:294–343
27. Gozem S, Luk HL, Schapiro I, Olivucci M. 2017. Theory and Simulation of the Ultrafast Double-Bond Isomerization of Biological Chromophores. *Chem. Rev.* 117:13502–13565
28. Oberhofer H, Reuter K, Blumberger J. 2017. Charge Transport in Molecular Materials: An Assessment of Computational Methods. *Chem. Rev.* 117:10319–10357
29. Morzan UN, de Armiño DJA, Foglia NO, Lebrero MCG, Scherlis DA, Estrin DA. 2018. Spectroscopy in Complex Environments from QM–MM Simulations. *Chem. Rev.* 118:4071–4113
30. Boulanger E, Harvey JN. 2018. QM/MM methods for free energies and photochemistry. *Curr. Opin. Struct. Biol.* 49:72–76
31. Mennucci B, Corni S. 2019. Multiscale modelling of photoinduced processes in composite systems. *Nat. Rev. Chem.* 2:1
32. Segatta F, Cupellini L, Garavelli M, Mennucci B. 2019. Quantum Chemical Modeling of the Photoinduced Activity of Multichromophoric Biosystems. *Chem. Rev.* 119:9361–9380
33. Nelson TR, White AJ, Bjorgaard JA, Sifain AE, Zhang Y, et al. 2020. Non-adiabatic Excited-State Molecular Dynamics: Theory and Applications for Modeling Photophysics in Extended Molecular Materials. *Chem. Rev.* 120:2215–2287
34. Curutchet C, Muñoz-Losa A, Monti S, Kongsted J, Scholes GD, Mennucci B. 2009. Electronic Energy Transfer in Condensed Phase Studied by a Polarizable QM/MM Model. *J. Chem. Theory Comput.* 5:1838–1848
35. Olsen JMH, Kongsted J. 2011. Molecular Properties through Polarizable Embedding. In *Ad-*

vances in Quantum Chemistry, eds. JR Sabin, E Brndas. Elsevier, 107–143
36. Dziedzic J, Mao Y, Shao Y, Ponder J, Head-Gordon T, et al. 2016. TINKTEP: A fully self-consistent, mutually polarizable QM/MM approach based on the AMOEBA force field. *J. Chem. Phys.* 145:124106
37. Vitale V, Dziedzic J, Albaugh A, Niklasson AMN, Head-Gordon T, Skylaris CK. 2017. Performance of extended Lagrangian schemes for molecular dynamics simulations with classical polarizable force fields and density functional theory. *J. Chem. Phys.* 146:124115
38. Boulanger E, Thiel W. 2012. Solvent Boundary Potentials for Hybrid QM/MM Computations Using Classical Drude Oscillators: A Fully Polarizable Model. *J. Chem. Theory Comput.* 8:4527–4538
39. Sahoo SK, Nair NN. 2018. Interfacing the Core-Shell or the Drude Polarizable Force Field With Car–Parrinello Molecular Dynamics for QM/MM Simulations. *Front. Chem.* 6:275
40. Lemkul JA, Huang J, Roux B, MacKerell Jr. AD. 2016. An Empirical Polarizable Force Field Based on the Classical Drude Oscillator Model: Development History and Recent Applications. *Chem. Rev.* 116:4983–5013
41. Lipparini F, Scalmani G, Mennucci B, Cancès E, Caricato M, Frisch MJ. 2010. A variational formulation of the polarizable continuum model. *J. Chem. Phys.* 133:014106
42. Loco D, Lagardère L, Cisneros GA, Scalmani G, Frisch M, et al. 2019. Towards large scale hybrid QM/MM dynamics of complex systems with advanced point dipole polarizable embeddings. *Chem. Sci.* 10:7200–7211
43. Lipparini F, Stamm B, Cancès E, Maday Y, Mennucci B. 2013. Fast Domain Decomposition Algorithm for Continuum Solvation Models: Energy and First Derivatives. *J. Chem. Theory Comput.* 9:3637–3648
44. Lipparini F, Lagardère L, Raynaud C, Stamm B, Cancès E, et al. 2015. Polarizable Molecular Dynamics in a Polarizable Continuum Solvent. *J. Chem. Theory Comput.* 11:623–634
45. Rappe AK, Goddard III WA. 1991. Charge equilibration for molecular dynamics simulations. *J. Phys. Chem.* 95:3358–3363
46. Rick SW, Stuart SJ, Berne BJ. 1994. Dynamical fluctuating charge force fields: Application to liquid water. *J. Chem. Phys.* 101:6141–6156
47. Klamt A, Schuurmann G. 1993. COSMO: a new approach to dielectric screening in solvents with explicit expressions for the screening energy and its gradient. *J. Chem. Soc., Perkin Trans. 2* :799–805
48. York, DM and Karplus, M. 1999. A smooth solvation potential based on the conductor-like screening model. *J. Phys. Chem. A* 103:11060–11079
49. Lipparini F, Scalmani G, Mennucci B, Frisch MJ. 2011. Self-Consistent Field and Polarizable Continuum Model: A New Strategy of Solution for the Coupled Equations. *J. Chem. Theory Comput.* 7:610–617
50. Casida ME, Jamorski C, Casida KC, Salahub DR. 1998. Molecular excitation energies to high-lying bound states from time-dependent density-functional response theory: Characterization and correction of the time-dependent local density approximation ionization threshold. *J. Chem. Phys.* 108:4439–4449
51. Caricato M, Mennucci B, Tomasi J, Ingrosso F, Cammi R, et al. 2006. Formation and relaxation of excited states in solution: A new time dependent polarizable continuum model based on time dependent density functional theory. *J. Chem. Phys.* 124:124520
52. Lipparini F, Cappelli C, Barone V. 2012. Linear response theory and electronic transition energies for a fully polarizable QM/Classical Hamiltonian. *J. Chem. Theory Comput.* 8:4153–4165
53. Cammi R, Tomasi J. 1995. Nonequilibrium solvation theory for the polarizable continuum model: A new formulation at theSCF level with application to the case of the frequency-dependent linear electric response function. *Int. J. Quantum Chem.* 56:465–474
54. Corni S, Cammi R, Mennucci B, Tomasi J. 2005. Electronic excitation energies of molecules

in solution within continuum solvation models: Investigating the discrepancy between state-specific and linear-response methods. *J. Chem. Phys.* 123:134512–10
55. Lunkenheimer, Bernd and Köhn, Andreas. 2013. Solvent Effects on Electronically Excited States Using the Conductor-Like Screening Model and the Second-Order Correlated Method ADC(2). *J. Chem. Theory Comput.* 9:977–994
56. Schwabe T. 2016. General theory for environmental effects on (vertical) electronic excitation energies. *J. Chem. Phys.* 145:154105–7
57. Improta, Roberto and Barone, Vincenzo and Scalmani, Giovanni and Frisch, Michael J. 2006. A state-specific polarizable continuum model time dependent density functional theory method for excited state calculations in solution. *J. Chem. Phys.* 125:054103
58. Marenich AV, Cramer CJ, Truhlar DG, Guido CA, Mennucci B, et al. 2011. Practical computation of electronic excitation in solution: vertical excitation model. *Chem. Sci.* 2:2143–2161
59. Lipparini F, Mennucci B. 2016. Perspective: Polarizable continuum models for quantum-mechanical descriptions. *J. Chem. Phys.* 144:160901
60. Guido CA, Jacquemin D, Adamo C, Mennucci B. 2015. Electronic Excitations in Solution: The Interplay between State Specific Approaches and a Time-Dependent Density Functional Theory Description. *J. Chem. Theory Comput.* 11:5782–5790
61. Caricato M. 2018. Coupled cluster theory with the polarizable continuum model of solvation. *Int. J. Quantum Chem.* 119:e25710
62. Cammi R, Frediani L, Mennucci B, Tomasi J, Ruud K, Mikkelsen KV. 2002. A second-order, quadratically convergent multiconfigurational self-consistent field polarizable continuum model for equilibrium and nonequilibrium solvation. *J. Chem. Phys.* 117:13–26
63. Cammi R, Frediani L, Mennucci B, Ruud K. 2003. Multiconfigurational self-consistent field linear response for the polarizable continuum model: Theory and application to ground and excited-state polarizabilities of para-nitroaniline in solution. *J. Chem. Phys.* 119:5818–5827
64. Li Q, Mennucci B, Robb MA, Blancafort L, Curutchet C. 2015. Polarizable QM/MM Multiconfiguration Self-Consistent Field Approach with State-Specific Corrections: Environment Effects on Cytosine Absorption Spectrum. *J. Chem. Theory Comput.* 11:1674–1682
65. Olsen J, Jo/rgensen P. 1985. Linear and nonlinear response functions for an exact state and for an MCSCF state. *J. Chem. Phys.* 82:3235–3264
66. Delcey MG, Pedersen TB, Aquilante F, Lindh R. 2015. Analytical gradients of the state-average complete active space self-consistent field method with density fitting. *J. Chem. Phys.* 143:044110
67. Furche F, Ahlrichs R. 2002. Adiabatic time-dependent density functional methods for excited state properties. *J. Chem. Phys.* 117:7433–7447
68. Scalmani G, Frisch MJ, Mennucci B, Tomasi J, Cammi R, Barone V. 2006. Geometries and properties of excited states in the gas phase and in solution: Theory and application of a time-dependent density functional theory polarizable continuum model. *J. Chem. Phys.* 124:094107
69. Carnimeo I, Cappelli C, Barone V. 2015. Analytical gradients for MP2, double hybrid functionals, and TD-DFT with polarizable embedding described by fluctuating charges. *J. Comput. Chem.* 36:2271–2290
70. Menger MFSJ, Caprasecca S, Mennucci B. 2017. Excited-State Gradients in Polarizable QM/MM Models: An Induced Dipole Formulation. *J. Chem. Theory Comput.* 13:3778–3786
71. Nottoli M, Mennucci B, Lipparini F. 2020. Excited state born-oppenheimer molecular dynamics through a coupling between time dependent DFT and AMOEBA. *Phys. Chem. Chem. Phys.*
72. R. Cammi. 2009. Quantum cluster theory for the polarizable continuum model. I. The CCSD level with analytical first and second derivatives. *J. Chem. Phys.* 131:164104
73. Caricato M. 2019. CCSD-PCM Excited State Energy Gradients with the Linear Response Singles Approximation to Study the Photochemistry of Molecules in Solution. *ChemPhotoChem* 3:747–754

74. Khani SK, Khah AM, Httig C. 2018. COSMO-RI-ADC(2) excitation energies and excited state gradients. *Phys. Chem. Chem. Phys.* 20:16354–16363
75. Khah AM, Khani SK, Httig C. 2018. Analytic Excited State Gradients for the QM/MM Polarizable Embedded Second-Order Algebraic Diagrammatic Construction for the Polarization Propagator PE-ADC(2). *J. Chem. Theory Comput.* 14:4640–4650
76. Lasorne B, Worth GA, Robb MA. 2011. Excited-state dynamics. *Wiley Interdiscip. Rev.: Comput. Mol. Sci.* 1:460–475
77. Markland TE, Ceriotti M. 2018. Nuclear quantum effects enter the mainstream. *Nat. Rev. Chem.* 2
78. Hammes-Schiffer S. 2020. Quantum effects in complex systems: summarizing remarks. *Faraday Discuss.* 221:582–588
79. Mai S, Gattuso H, Monari A, González L. 2018. Novel Molecular-Dynamics-Based Protocols for Phase Space Sampling in Complex Systems. *Front. Chem.* 6
80. Hammes-Schiffer S, Tully JC. 1994. Proton transfer in solution: Molecular dynamics with quantum transitions. *J. Chem. Phys.* 101:4657–4667
81. Crespo-Otero R, Barbatti M. 2018. Recent Advances and Perspectives on Nonadiabatic Mixed Quantum–Classical Dynamics. *Chem. Rev.* 118:7026–7068
82. Ibele LM, Curchod BFE. 2020. A molecular perspective on Tully models for nonadiabatic dynamics. *Phys. Chem. Chem. Phys.* 22:15183–15196
83. Nelson TR, White AJ, Bjorgaard JA, Sifain AE, Zhang Y, et al. 2020. Non-adiabatic Excited-State Molecular Dynamics: Theory and Applications for Modeling Photophysics in Extended Molecular Materials. *Chem. Rev.* 120:2215–2287
84. Tully JC, Preston RK. 1971. Trajectory Surface Hopping Approach to Nonadiabatic Molecular Collisions: The Reaction of H^+ with D2. *J. Chem. Phys.* 55:562–572
85. Tully JC. 1990. Molecular dynamics with electronic transitions. *J. Chem. Phys.* 93:1061–1071
86. Persico M, Granucci G. 2014. An overview of nonadiabatic dynamics simulations methods, with focus on the direct approach versus the fitting of potential energy surfaces. *Theor. Chem. Acc.* 133:1526
87. Wang L, Long R, Prezhdo OV. 2015. Time-Domain Ab Initio Modeling of Photoinduced Dynamics at Nanoscale Interfaces. *Annu. Rev. Phys. Chem.* 66:549–579
88. Wang L, Akimov A, Prezhdo OV. 2016. Recent Progress in Surface Hopping: 2011–2015. *J. Phys. Chem. Lett.* 7:2100–2112
89. Granucci G, Persico M, Toniolo A. 2001. Direct semiclassical simulation of photochemical processes with semiempirical wave functions. *J. Chem. Phys.* 114:10608–10615
90. Mandal A, Yamijala SS, Huo P. 2018. Quasi-Diabatic Representation for Nonadiabatic Dynamics Propagation. *J. Chem. Theory Comput.* 14:1828–1840
91. Plasser F, Granucci G, Pittner J, Barbatti M, Persico M, Lischka H. 2012. Surface hopping dynamics using a locally diabatic formalism: Charge transfer in the ethylene dimer cation and excited state dynamics in the 2-pyridone dimer. *J. Chem. Phys.* 137:22A514
92. Mai S, Marquetand P, González L. 2018. Nonadiabatic dynamics: The SHARC approach. *Wiley Interdiscip. Rev.: Comput. Mol. Sci.* 8:e1370
93. Linjun Wang and Jing Qiu and Xin Bai and Jiabo Xu. 2019. Surface hopping methods for nonadiabatic dynamics in extended systems. *Wires Comput. Mol. Sci.* 10:1435
94. Aguilera-Porta N, Corral I, Munoz-Muriedas J, Granucci G. 2019. Excited state dynamics of some nonsteroidal anti-inflammatory drugs: A surface-hopping investigation. *Comput. Theor. Chem.* 1152:20–27
95. Persico M, Granucci G. 2018. Photochemistry: A Modern Theoretical Perspective. Springer, Cham (Switzerland)
96. Plasser F, Mai S, Fumanal M, Gindensperger E, Daniel C, González L. 2019. Strong Influence of Decoherence Corrections and Momentum Rescaling in Surface Hopping Dynamics of Transition Metal Complexes. *J. Chem. Theory Comput.* 15:5031–5045

97. Subotnik JE, Jain A, Landry B, Petit A, Ouyang W, Bellonzi N. 2016. Understanding the Surface Hopping View of Electronic Transitions and Decoherence. *Annu. Rev. Phys. Chem.* 67:387–417
98. Granucci G, Persico M, Zoccante A. 2010. Including quantum decoherence in surface hopping. *J. Chem. Phys.* 133:134111
99. Jaeger HM, Fischer S, Prezhdo OV. 2012. Decoherence-induced surface hopping. *J. Chem. Phys.* 137:22A545
100. Nelson T, Fernandez-Alberti S, Roitberg AE, Tretiak S. 2013. Nonadiabatic excited-state molecular dynamics: Treatment of electronic decoherence. *J. Chem. Phys.* 138:224111
101. Ha JK, Lee IS, Min SK. 2018. Surface Hopping Dynamics beyond Nonadiabatic Couplings for Quantum Coherence. *J. Phys. Chem. Lett.* 9:1097–1104
102. Gao X, Thiel W. 2017. Non-Hermitian surface hopping. *Phys. Rev. E* 95:013308
103. Zhou P, Han K. 2018. Unraveling the Detailed Mechanism of Excited-State Proton Transfer. *Acc. Chem. Res.* 51:1681–1690
104. Vendrell O, Moreno M, Lluch JM, Hammes-Schiffer S. 2004. Molecular Dynamics of Excited State Intramolecular Proton Transfer: 2-(2‘-Hydroxyphenyl)-4-methyloxazole in Gas Phase, Solution, and Protein Environments†. *J. Phys. Chem. B* 108:6616–6623
105. Bellucci MA, Coker DF. 2012. Molecular dynamics of excited state intramolecular proton transfer: 3-hydroxyflavone in solution. *J. Chem. Phys.* 136:194505
106. Tolbert LM, Solntsev KM. 2002. Excited-state proton transfer: from constrained systems to "super" photoacids to superfast proton transfer. *Acc. Chem. Res.* 35:19–27
107. Domcke W, Sobolewski AL. 2003. Chemistry. Unraveling the molecular mechanisms of photoacidity. *Sci.* 302:1693–1694
108. Hynes JT. 2015. Molecules in motion: Chemical reaction and allied dynamics in solution and elsewhere. *Annu. Rev. Phys. Chem.* 66:1–20
109. Raucci U, Savarese M, Adamo C, Ciofini I, Rega N. 2015. Intrinsic and Dynamical Reaction Pathways of an Excited State Proton Transfer. *J. Phys. Chem. B* 119:2650–2657
110. Chiariello MG, Rega N. 2018. Exploring Nuclear Photorelaxation of Pyranine in Aqueous Solution: an Integrated Ab-Initio Molecular Dynamics and Time Resolved Vibrational Analysis Approach. *J. Phys. Chem. A* 122:2884–2893
111. David Casanova. 2018. Theoretical Modeling of Singlet Fission. *Chem. Rev.* 118:7164–7207
112. Kiyoshi Miyata and Felisa S. Conrad-Burton and Florian L. Geyer and X.-Y. Zhu. 2019. Triplet Pair States in Singlet Fission. *Chem. Rev.* 119:4261–4292
113. Alexey V. Akimov and Oleg V. Prezhdo. 2014. Nonadiabatic Dynamics of Charge Transfer and Singlet Fission at the Pentacene/C60 Interface. *J. Am. Chem. Soc.* 136:1599–1608
114. Accomasso D, Granucci G, Wibowo M, Persico M. 2020. Delocalization effects in singlet fission: Comparing models with two and three interacting molecules. *J. Chem. Phys.* 152:244125
115. Ding F, Lingerfelt DB, Mennucci B, Li X. 2015. Time-dependent non-equilibrium dielectric response in QM/continuum approaches. *J. Chem. Phys.* 142:034120
116. Corni S, Pipolo S, Cammi R. 2015. Equation of Motion for the Solvent Polarization Apparent Charges in the Polarizable Continuum Model: Application to Real-Time TDDFT. *J. Phys. Chem. A* 119:5405–5416
117. Wu X, Teuler JM, Cailliez F, Clavaguéra C, Salahub DR, de la Lande A. 2017. Simulating Electron Dynamics in Polarizable Environments. *J. Chem. Theory Comput.* 13:3985–4002
118. Wildman A, Donati G, Lipparini F, Mennucci B, Li X. 2019. Nonequilibrium Environment Dynamics in a Frequency-Dependent Polarizable Embedding Model. *J. Chem. Theory Comput.* 15:43–51
119. Lu Z, Zhang Y. 2008. Interfacing ab Initio Quantum Mechanical Method with Classical Drude Osillator Polarizable Model for Molecular Dynamics Simulation of Chemical Reactions. *J. Chem. Theory Comput.* 4:1237–1248
120. Schwörer M, Breitenfeld B, Tröster P, Bauer S, Lorenzen K, et al. 2013. Coupling density

functional theory to polarizable force fields for efficient and accurate Hamiltonian molecular dynamics simulations. *J. Chem. Phys.* 138:244103–14
121. Hagras MA, Glover WJ. 2018. Polarizable Embedding for Excited-State Reactions: Dynamically Weighted Polarizable QM/MM. *J. Chem. Theory Comput.* 14:2137–2144
122. Sisto A, Stross C, van der Kamp MW, O'Connor M, McIntosh-Smith S, et al. 2017. Atomistic non-adiabatic dynamics of the LH2 complex with a GPU-accelerated ab initio exciton model. *Phys. Chem. Chem. Phys.* 19:14924–14936
123. Maximilian F. S. J. Menger and Felix Plasser and Benedetta Mennucci and Leticia González. 2018. Surface Hopping within an Exciton Picture. An Electrostatic Embedding Scheme. *J. Chem. Theory Comput.* 14:6139–6148
124. Segatta F, Cupellini L, Garavelli M, Mennucci B. 2019. Quantum Chemical Modeling of the Photoinduced Activity of Multichromophoric Biosystems. *Chem. Rev.* 119:9361–9380
125. Hsu CP, Fleming GR, Head-Gordon M, Head-Gordon T. 2001. Excitation energy transfer in condensed media. *J. Chem. Phys.* 114:3065–3072
126. Curutchet C, Kongsted J, Muñoz-Losa A, Hossein-Nejad H, Scholes GD, Mennucci B. 2011. Photosynthetic Light-Harvesting Is Tuned by the Heterogeneous Polarizable Environment of the Protein. *J. Am. Chem. Soc.* 133:3078–3084
127. Iozzi MF, Mennucci B, Tomasi J, Cammi R. 2004. Excitation energy transfer (EET) between molecules in condensed matter: A novel application of the polarizable continuum model (PCM). *J. Chem. Phys.* 120:7029–7040
128. Madjet ME, Abdurahman A, Renger T. 2006. Intermolecular Coulomb Couplings from Ab Initio Electrostatic Potentials: Application to Optical Transitions of Strongly Coupled Pigments in Photosynthetic Antennae and Reaction Centers. *J. Phys. Chem. B* 110:17268–17281
129. Dognon JP, Durand S, Granucci G, Lévy B, Millié P, Rabbe C. 2000. Atomic charges for molecular dynamics calculations. *J. Mol. Struct.: Theochem* 507:17–23
130. Spencer J, Gajdos F, Blumberger J. 2016. FOB-SH: Fragment orbital-based surface hopping for charge carrier transport in organic and biological molecules and materials. *J. Chem. Phys.* 145:064102
131. Giannini S, Carof A, Blumberger J. 2018. Crossover from Hopping to Band-Like Charge Transport in an Organic Semiconductor Model: Atomistic Nonadiabatic Molecular Dynamics Simulation. *J. Phys. Chem. Lett.* 9:3116–3123
132. May V, Kuhn O. 2011. Charge and Energy Transfer Dynamics in Molecular Systems. Weinheim, Germany: Wiley-VCH, 3rd ed.
133. Mukamel S. 1995. Principles of Nonlinear Optical Spectroscopy. New York: Oxford University Press
134. Valleau S, Eisfeld A, Aspuru-Guzik A. 2012. On the alternatives for bath correlators and spectral densities from mixed quantum-classical simulations. *J. Chem. Phys.* 137:224103
135. Yuri Georgievskii and Chao-Ping Hsu and R. A. Marcus. 1999. Linear response in theory of electron transfer reactions as an alternative to the molecular harmonic oscillator model. *J. Chem. Phys.* 110:5307–5317
136. Makri N. 1999. The Linear Response Approximation and Its Lowest Order Corrections: An Influence Functional Approach. *J. Phys. Chem. B* 103:2823–2829
137. Chenu A, Scholes GD. 2015. Coherence in Energy Transfer and Photosynthesis. *Annu. Rev. Phys. Chem.* 66:69–96
138. Jang SJ, Mennucci B. 2018. Delocalized excitons in natural light-harvesting complexes. *Rev. Mod. Phys.* 90:035003
139. Yang M, Fleming GR. 2002. Influence of phonons on exciton transfer dynamics: comparison of the Redfield, Frster, and modified Redfield equations. *Chem. Phys.* 275:355–372
140. Beljonne D, Curutchet C, Scholes GD, Silbey RJ. 2009. Beyond Forster Resonance Energy Transfer in Biological and Nanoscale Systems. *J. Phys. Chem. B* 113:6583–6599
141. Borrelli R, Peluso A. 2011. The temperature dependence of radiationless transition rates from

ab initio computations. *Phys. Chem. Chem. Phys.* 13:4420
142. Lee MH, Dunietz BD, Geva E. 2013. Calculation from First Principles of Intramolecular Golden-Rule Rate Constants for Photo-Induced Electron Transfer in Molecular Donor–Acceptor Systems. *J. Phys. Chem. C* 117:23391–23401
143. Borrelli R, Peluso A. 2013. Elementary electron transfer reactions: from basic concepts to recent computational advances. *Wiley Interdiscip. Rev.: Comput. Mol. Sci.* 3:542–559
144. Blumberger J. 2015. Recent Advances in the Theory and Molecular Simulation of Biological Electron Transfer Reactions. *Chem. Rev.* 115:11191–11238
145. Xueyu Song and R. A. Marcus. 1993. Quantum correction for electron transfer rates. Comparison of polarizable versus nonpolarizable descriptions of solvent. *J. Chem. Phys.* 99:7768–7773
146. Jortner J. 1976. Temperature dependent activation energy for electron transfer between biological molecules. *J. Chem. Phys.* 64:4860–4867
147. Cupellini L, Corbella M, Mennucci B, Curutchet C. 2018. Electronic energy transfer in biomacromolecules. *Wires Comput. Mol. Sci.* 9:e1392
148. You ZQ, Hsu CP. 2013. Theory and calculation for the electronic coupling in excitation energy transfer. *Int. J. Quantum Chem.* 114:102–115
149. Hsu CP, You ZQ, Chen HC. 2008. Characterization of the Short-Range Couplings in Excitation Energy Transfer. *J. Phys. Chem. C* 112:1204–1212
150. Hsu CP. 2009. The Electronic Couplings in Electron Transfer and Excitation Energy Transfer. *Acc. Chem. Res.* 42:509–518
151. You ZQ, Hsu CP. 2010. The fragment spin difference scheme for triplet-triplet energy transfer coupling. *J. Chem. Phys.* 133:074105
152. Azarias C, Russo R, Cupellini L, Mennucci B, Jacquemin D. 2017. Modeling excitation energy transfer in multi-BODIPY architectures. *Phys. Chem. Chem. Phys.* 19:6443–6453
153. Di Donato M, Iagatti A, Lapini A, Foggi P, Cicchi S, et al. 2014. Combined Experimental and Theoretical Study of Efficient and Ultrafast Energy Transfer in a Molecular Dyad. *J. Phys. Chem. C* 118:23476–23486
154. Troisi A, Orlandi G. 2001. The hole transfer in DNA: calculation of electron coupling between close bases. *Chem. Phys. Lett.* 344:509–518
155. Harcourt RD, Scholes GD, Ghiggino KP. 1994. Rate expressions for excitation transfer. II. Electronic considerations of direct and through–configuration exciton resonance interactions. *J. Chem. Phys.* 101:10521–10525
156. Voityuk AA, Rösch N. 2002. Fragment charge difference method for estimating donor–acceptor electronic coupling: Application to DNA π-stacks. *J. Chem. Phys.* 117:5607–5616
157. Voityuk AA. 2013. Estimation of Electronic Coupling for Photoinduced Charge Separation and Charge Recombination Using the Fragment Charge Difference Method. *J. Phys. Chem. C* 117:2670–2675
158. Yang CHY, Hsu CP. 2013. A multi-state fragment charge difference approach for diabatic states in electron transfer: Extension and automation. *J. Chem. Phys.* 139:154104
159. Efrima S, Bixon M. 1976. Vibrational effects in outer-sphere electron-transfer reactions in polar media. *Chem. Phys.* 13:447–460
160. Vaissier V, Barnes P, Kirkpatrick J, Nelson J. 2013. Influence of polar medium on the reorganization energy of charge transfer between dyes in a dye sensitized film. *Phys. Chem. Chem. Phys.* 15:4804
161. Cupellini L, Giannini S, Mennucci B. 2018. Electron and excitation energy transfers in covalently linked donor–acceptor dyads: mechanisms and dynamics revealed using quantum chemistry. *Phys. Chem. Chem. Phys.* 20:395–403
162. Blumberger J. 2008. Free energies for biological electron transfer from QM/MM calculation: method, application and critical assessment. *Phys. Chem. Chem. Phys.* 10:5651
163. Cupellini L, Calvani D, Jacquemin D, Mennucci B. 2020. Charge transfer from the carotenoid can quench chlorophyll excitation in antenna complexes of plants. *Nat. Comm.* 11:662

164. Stasyuk AJ, Stasyuk OA, Solà M, Voityuk AA. 2019. Photoinduced electron transfer and unusual environmental effects in fullerene–Zn-porphyrin–BODIPY triads. *Phys. Chem. Chem. Phys.* 21:25098–25107
165. Iagatti A, Cupellini L, Biagiotti G, Caprasecca S, Fedeli S, et al. 2016. Efficient photoinduced charge separation in a BODIPY–c60 dyad. *J. Phys. Chem. C* 120:16526–16536
166. Botu V, Batra R, Chapman J, Ramprasad R. 2017. Machine learning force fields: construction, validation, and outlook. *J. Phys. Chem. C* 121:511–522
167. Dral PO. 2020. Quantum Chemistry in the Age of Machine Learning. *J. Phys. Chem. Lett.* 11:2336–2347